NRF1-mediated mitochondrial biogenesis antagonizes innate antiviral immunity

Tian Zhao[1], Jiaojiao Zhang[1], Hong Lei[1], Yuanyuan Meng[1], Hongcheng Cheng[1], Yanping Zhao[2], Guangfeng Geng[1], Chenglong Mu[1] (ID), Linbo Chen[1] (ID), Qiangqiang Liu[1] (ID), Qian Luo[1], Chuanmei Zhang[1], Yijia Long[1], Jingyi Su[1], Yinhao Wang[1], Zhuoya Li[1] (ID), Jiaxing Sun[1], Guo Chen[1], Yanjun Li[1], Xudong Liao[1], Yingli Shang[3], Gang Hu[2], Quan Chen[1] & Yushan Zhu[1,*] (ID)

Abstract

Mitochondrial biogenesis is the process of generating new mitochondria to maintain cellular homeostasis. Here, we report that viruses exploit mitochondrial biogenesis to antagonize innate antiviral immunity. We found that nuclear respiratory factor-1 (NRF1), a vital transcriptional factor involved in nuclear-mitochondrial interactions, is essential for RNA (VSV) or DNA (HSV-1) virus-induced mitochondrial biogenesis. NRF1 deficiency resulted in enhanced innate immunity, a diminished viral load, and morbidity in mice. Mechanistically, the inhibition of NRF1-mediated mitochondrial biogenesis aggravated virus-induced mitochondrial damage, promoted the release of mitochondrial DNA (mtDNA), increased the production of mitochondrial reactive oxygen species (mtROS), and activated the innate immune response. Notably, virus-activated kinase TBK1 phosphorylated NRF1 at Ser318 and thereby triggered the inactivation of the NRF1-TFAM axis during HSV-1 infection. A knock-in (KI) strategy that mimicked TBK1-NRF1 signaling revealed that interrupting the TBK1-NRF1 connection ablated mtDNA release and thereby attenuated the HSV-1-induced innate antiviral response. Our study reveals a previously unidentified antiviral mechanism that utilizes a NRF1-mediated negative feedback loop to modulate mitochondrial biogenesis and antagonize innate immune response.

Introduction

In metazoans, crosstalk between the major organelles and innate immune signaling during infection is critical for eliminating pathogens and maintaining tissue homeostasis. Mitochondria are functionally versatile organelles that have demonstrated activity in the regulation of innate immunity during microbial invasion, involving multiple mechanisms (Weinberg *et al*, 2015; Mills *et al*, 2017). Components of mitochondria, such as mitochondrial DNA (mtDNA) and mitochondrial reactive oxygen species (mtROS), are released in response to mitochondrial damage and act as danger-associated molecular patterns (DAMPs). These contribute to the formation of mitochondrial antiviral signaling protein (MAVS) complex and have been associated with the activation of NLRP3 inflammasome (Seth *et al*, 2005; Zhang *et al*, 2010; Zhong *et al*, 2018). Viral infection inevitably results in mitochondrial damage in hosts, and mitochondrial DAMPs derived from damaged mitochondria are the driving force of innate antiviral immunity. Studies have shown that some viruses can manipulate various steps of the molecular machinery of mitophagy to remove damaged mitochondria for their own benefit (Kim *et al*, 2013; Khan *et al*, 2016; Burman *et al*, 2017).

Considered a major contributing factor to innate immunity, mitochondrial quality control occurs via various mechanisms, including mitophagy, mitochondrial dynamics, proteostasis, and mitochondrial biogenesis. Mitophagy is a selective form of autophagy and functions to prevent the accumulation of damaged mitochondria that could cause excessive innate immune responses (Cho *et al*, 2020; Xu *et al*, 2020). Mitochondrial dynamics adapt rapidly to manage the balance between mitochondrial fusion and fission, which is associated with improved mtROS production, mitochondrial metabolism, and mitophagy (Sprenger & Langer, 2019; Chen *et al*, 2020). The reprogramming of mitochondrial metabolism dictates the maturation, migration, and function of various innate immune cells through metabolic intermediates such as succinate, fumarate, and

1   State Key Laboratory of Medicinal Chemical Biology, Frontiers Science Center for Cell Responses, Tianjin Key Laboratory of Protein Science, College of Life Sciences, Nankai University, Tianjin, China
2   School of Statistics and Data Science, LPMC and KLMDASR, Nankai University, Tianjin, China
3   Department of Preventive Veterinary Medicine, College of Veterinary Medicine, Shandong Agricultural University, Taian, China
    *Corresponding author. Tel: +86 22 23502962; E-mail: zhuys@nankai.edu.cn

itaconate (Tannahill *et al*, 2013; Kornberg *et al*, 2018; Mills *et al*, 2018; Humphries *et al*, 2020). Mitochondrial proteostasis also has a role in the aspect of antibacterial host defense (Pellegrino *et al*, 2014). Despite the ultimate importance of these quality control processes in regulating innate immunity, it remains unclear how mitochondrial biogenesis is regulated in response to pathogens' invasion.

Mitochondrial biogenesis is dependent on the timely and coordinated transcriptional control of both mitochondrial-encoded and nuclear-encoded genes (Attardi & Schatz, 1988). The protein-coding capacity of the mitochondrial genome is limited to 13 respiratory subunits. Thus, nuclear genes provide the vast majority of gene products required for the biochemical functions and molecular architecture of mitochondria (Scarpulla *et al*, 2012). The expression of nuclear-encoded mitochondrial genes (NEMGs) was shown to be regulated by multiple transcriptional factors, including nuclear respiratory factor (NRF) 1, NRF2 (also known as GABP), estrogen-related receptor alpha (ERRα), peroxisome proliferator-activated receptor-α (PPARα), and c-Myc (Virbasius *et al*, 1993; Vega *et al*, 2000; Vercauteren *et al*, 2008; Eichner & Giguere, 2011; Lee *et al*, 2017). In addition, the PPARγ coactivator (PGC)-1 family of regulated coactivators (PGC1-α, PGC1-β, PRC) also exert their effects on the expression of NEMGs through interacting with these transcriptional factors (Scarpulla, 2008).

NRF1 and NRF2, which are distinct from *NFE2L1* (nuclear factor, erythroid 2 like 1) and *NFE2L2* (nuclear factor, erythroid 2 like 2) genes responsible for ROS detoxification, although they share the same names in bibliographic databases, have been found to transcriptionally regulate many mammalian nuclear genes whose products function in the mitochondria (Scarpulla, 1996). They are able to promote the expression of respiratory subunits that comprise all five of the mitochondrial respiratory complexes, as well as assembly factors, parts of mitochondrial transcription and translation machinery, and auxiliary factors (TFAM, TFB1M, TFB2M) necessary for mtDNA maintenance and stability (Kelly & Scarpulla, 2004; Scarpulla, 2012). Through activating mitochondrial biogenesis, NRF1 and NRF2 are capable of regulating many biological processes, including cell metabolism, cell proliferation and differentiation, aging, and tumorigenesis (Mohrin *et al*, 2015; Luo *et al*, 2017; Chow *et al*, 2019; Ma *et al*, 2019). However, it remains largely unknown whether and how NRFs-mediated mitochondrial biogenesis responds to viral infection and further regulates innate antiviral immunity.

In this study, we identified a role for NRF1 in mediating mitochondrial biogenesis that was essential for regulating innate antiviral immunity. RNA virus and DNA virus activated NRF1-mediated mitochondrial biogenesis, which subsequently acted to inhibit mitochondrial damage and reduced excessive activation of the innate antiviral response by mitochondrial DAMPs. Consistently, NRF1 deficiency enhanced virus-induced innate antiviral immunity *in vitro* and *in vivo* and NRF1-deficient mice were more resistant to lethal viral infection compared with the wild-type controls. Furthermore, we also identified NRF1 as a substrate of TBK1 kinase during HSV-1 infection. Ablation of TBK1-mediated phosphorylation of NRF1 specifically enhanced TFAM activity, which subsequently inhibited innate antiviral response through attenuating mtDNA stress. Therefore, our findings describe a crucial role for NRF1-mediated mitochondrial biogenesis in the innate antiviral immunity and highlight a vital link connecting innate immunity to mitochondrial quality control.

Results

Viral infection activates NRF1-mediated mitochondrial biogenesis

To investigate whether NRFs-mediated mitochondrial biogenesis occurs during viral infection, we first analyzed the expression of NRF1, NRF2-α, and PGC1-α in mouse peritoneal macrophages (PMs) and human monocytic leukemia (THP-1) cells infected with vesicular stomatitis virus (VSV, RNA virus) or herpes simplex virus 1 (HSV-1, DNA virus). Interestingly, only the protein level of NRF1 was markedly increased upon viral infection (Figs 1A and EV1A). Similar results were obtained from mouse PMs and human THP-1 cells stimulated with poly(I:C) or interferon-stimulatory DNA (ISD), which were considered mimics of double-stranded RNA or DNA, respectively (Figs 1A and EV1A). *Nrf1* mRNA levels were also substantially upregulated in mouse PMs after treatment with various stimuli to activate innate immunity (Fig 1B). Using gene

Figure 1. Viral infection activates NRF1-mediated mitochondrial biogenesis.

A   Immunoblot analysis of NRF1, NRF2-α, and PGC1-α in mouse PMs infected with VSV or HSV-1 or treated with poly(I:C) or ISD for the indicated time points. ACTIN was used as a loading control. Ratios of target proteins versus loading control normalized to the 0-h time point of each condition.

B   qPCR analysis of *Nrf1*, *Gabpa*, and *Ppargc1a* mRNA in mouse PMs infected with VSV or HSV-1 or treated with poly(I:C) or ISD for the indicated time points ($n = 3$ biological replicates per group).

C   Immunoblot analysis of NRF1 expression in mouse PMs transfected with p65-specific siRNA (si-p65) or control siRNA (si-NC) for 48 h, followed by infection with VSV or HSV-1 for 8 h. GAPDH was used as a loading control. Ratios of target proteins versus loading control normalized to the untreated sample of each condition.

D   qPCR analysis of *Nrf1* mRNA in mouse PMs transfected with p65-specific siRNA (si-p65) or control siRNA (si-NC) for 48 h, followed by infection with VSV or HSV-1 for 8 h ($n = 3$ biological replicates per group).

E   Immunoblot analysis of mitochondrial proteins and autophagy marker LC3 in mouse PMs transfected with NRF1-specific siRNA (si-NRF1) or control siRNA (si-NC) for 48 h, followed by infection with VSV or HSV-1 for the indicated time points. ACTIN was used as a loading control. Ratios of target proteins versus loading control normalized to the untreated sample of each condition.

F   Mitochondrial mass determined by mtDNA/nuclear DNA (nDNA) ratio in mouse PMs transfected with NRF1-specific siRNA (si-NRF1) or control siRNA (si-NC) for 48 h, followed by infection with VSV or HSV-1 for the indicated time points ($n = 3$ biological replicates per group).

Data information: Data are from three independent experiments (B, D, and F) or representative data (A, C, and E) and presented as mean ± s.e.m. ns, not significant ($P > 0.05$), *$P < 0.05$, **$P < 0.01$, ***$P < 0.001$, using a two-tailed, unpaired Student's *t*-test.
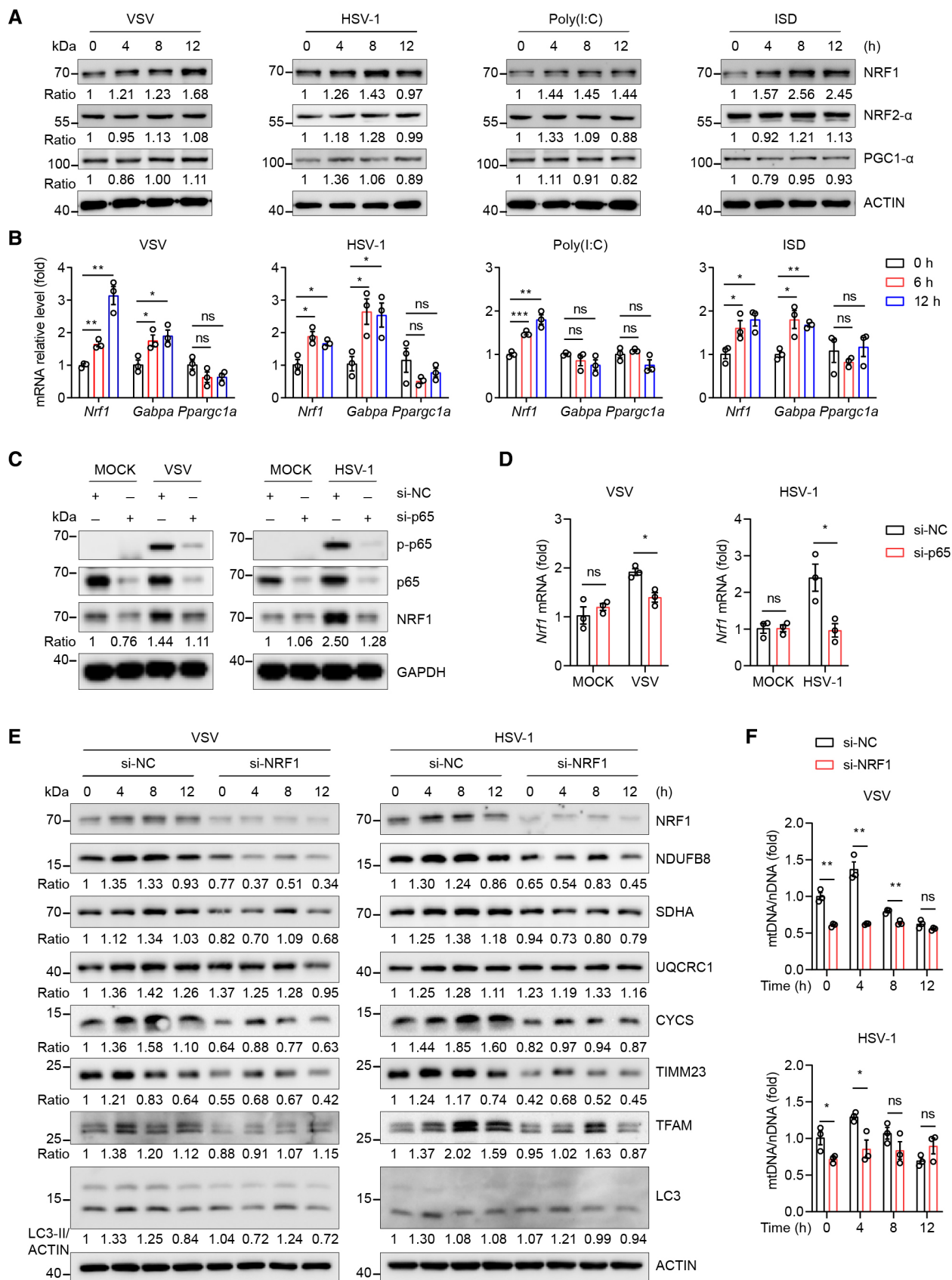Source data are available online for this figure.

Figure 1.

transcription profiling data available from GEO database, we indicated increased *NRF1* mRNA expression in Dengue-infected and hepatitis B virus (HBV)-infected patients (Fig EV1B). Consistent with the enhanced expression of NRF1 during viral infection, the fraction of dimerized NRF1 (activated form) was also significantly increased in VSV or HSV-1-infected mouse PMs and human THP-1 cells (Figs EV1C and EV1D). To further detect the effect of viral infection on the transcriptional activity of NRF1, we expressed luciferase reporters driven by NRF1 binding promoter regions of *TFAM* or *TFB1M* in HEK293T cells and found that VSV infection enhanced the NRF1-regulated promoter activities (Fig EV1E). Previously, it was reported that lipopolysaccharide (LPS) treatment induced NF-κB-dependent upregulation of NRF1 (Suliman *et al*, 2010). NF-κB is also activated in virus-trigged signaling, thus we sought to determine whether NRF1 was induced by NF-κB upon viral infection and found that inhibiting NF-κB with a p65-specific small interfering RNA (siRNA) (Fig 1C and D) or a IκB kinase inhibitor BAY 11-7082 (Appendix Fig S1A and B) significantly abrogated virus-induced upregulation of NRF1. These data demonstrated that viral infection induced the activation of NRF1 in a NF-κB-dependent manner.

To further explore whether the upregulation of *Nrf1* induces mitochondrial biogenesis, we next checked mitochondrial DNA (mtDNA) and mitochondrial proteins upon viral infection and found that VSV and HSV-1 induced an increase in the levels of mtDNA and the amounts of mitochondrial proteins in mouse PMs as early as 4 h after infection (Fig EV1F–H). Previous studies showed that viral infection also activated the mitophagy machinery to clear damaged mitochondria from host cells (Lei *et al*, 2012; He *et al*, 2019). Here, virus-induced decreases in mtDNA and mitochondrial proteins levels, accompanied by the increase of lipidated LC3 (LC3-II), were observed at 8 or 12 h after viral infection. However, unlike the decreases of mitochondrial protein and mtDNA at the late phase of viral infection, the mRNA levels of many nuclear-encoded mitochondrial genes (NEMGs), such as *Tfam*, *Cycs*, *Uqcrc1*, *Mrpl13*, and *Mrpl27*, were enhanced gradually during the course of a complete infection (Fig EV1I), indicating that mitophagy and mitochondrial biogenesis were cooperating to maintain a balanced mitochondrial pool in virus-infected macrophages. To determine the function of NRF1 in the virus-induced mitochondrial biogenesis, we used siRNA to silence *Nrf1* and found that virus-induced expression of mitochondrial proteins, such as NDUFB8, SDHA, and UQCRC1, were

significantly inhibited by NRF1 knockdown (Fig 1E). The copy number of mtDNA was also reduced markedly in NRF1-knockdown macrophages and was maintained at a significantly decreased level at 0- to 4-h postinfection with VSV or HSV-1 (Fig 1F). Thus, our data demonstrate that viral infection induced NRF1 activation, which suggests an important role in connecting mitochondrial biogenesis and innate immunity.

NRF1 deficiency aggravates virus-induced mitochondrial damage and primes innate immune response

To further explore the function of NRF1 in virus-triggered mitochondrial biogenesis, we generated myeloid-specific NRF1-deficient (*Nrf1^{F/F}Lyz2^{Cre}*, hereafter called *Nrf1^{MyeKO}*) mice (**Appendix Fig S2A and B**). We first analyzed whether NRF1 deficiency had an effect on the development and differentiation of immune cells. The results demonstrated that the percentages of immune cells in the spleen and thymus were similar in *Nrf1^{MyeKO}* mice and their *Nrf1^{F/F}* littermates, indicating that NRF1 might not be required for the development of various lymphocytes and myeloid cells (**Appendix Fig S2C–E**). To dig out the genes regulated by NRF1 upon viral infection, we conducted high-throughput transcriptome profiling using mouse PMs isolated from *Nrf1^{MyeKO}* mice (NRF1-KO PMs) and their *Nrf1^{F/F}* littermates (wild-type PMs) after 8 h of VSV infection. The volcano plot analysis showed 1,154 significant differentially expressed genes (DEGs) in total, and 385 genes were upregulated and 769 genes were downregulated in NRF1-KO PMs (Fig 2A). Gene Ontology Cellular Component (GO_CC) enrichment analysis with the downregulated DEGs showed that the "mitochondrial inner membrane" represented the most enriched term (Fig 2B). Of note is that many mitochondrial respiratory genes, such as *Ndufa8*, *Ndufb8*, *Ndufb11*, *Sdha*, *Sdhaf4*, and *Uqcrc1*, were impaired by NRF1 deficiency (Fig 2C), indicating an importance of NRF1 for the maintenance of mitochondrial respiration in macrophages.

To further determine the effect of NRF1 deficiency on mitochondria, we first analyzed mitochondrial quality in NRF1-KO PMs at steady state without pathogen invasion. The results showed that NRF1 deficiency induced a decrease in the transcript levels of many NEMGs (Fig EV2A). However, unlike the reduced mRNA expression, only the protein level of NDUFB8 (subunit of complex I) and mitochondrial complex I was decreased in NRF1-KO PMs (Fig EV2B;

Figure 2. NRF1 deficiency aggravates virus-induced mitochondrial damage.

A–C RNA-sequencing (RNA-seq) analysis of gene expression in wild-type and NRF1-KO mouse PMs (*n* = 3 biological replicates per group) infected with VSV for 8 h. (A) Volcano plot of the differentially expressed genes (DEGs, log₂FC > 0.5, *P*~adj~ < 0.05). Red and blue dots represent the significantly upregulated and downregulated genes in NRF1-KO mouse PMs, respectively. (B) Gene ontology (GO) enrichment analysis of downregulated DEGs in NRF1-KO mouse PMs. Results showing top 5 significantly enriched GO terms in cellular component (CC). (C) Pheatmap analysis showing downregulated DEGs encoding mitochondrial inner membrane proteins. TPM, transcripts per kilobase of exon model per million mapped reads.

D Mitochondrial mass determined by mtDNA/nuclear DNA (nDNA) ratio in wild-type and NRF1-KO mouse PMs infected with VSV or HSV-1 for the indicated time points (*n* = 3 biological replicates per group).

E Flow cytometric analysis of mitochondria status in wild-type and NRF1-KO mouse PMs infected with VSV or HSV-1 for 8 h. Gates represent cells with damaged mitochondria. Quantification of cells with damaged mitochondria (*n* = 3 biological replicates per group).

F, G The representative curves of oxygen consumption rate (OCR) in wild-type and NRF1-KO mouse PMs infected with VSV (F) or HSV-1 (G) for 8 h (*n* = 5 biological replicates per group). Oligomycin: 1 μM, FCCP: 4 μM, Rotenone: 1 μM. Quantification of basal and maximal OCR.

H, I Electron micrographs of mitochondria in wild-type and NRF1-KO mouse PMs infected with VSV or HSV-1 for 8 h. Scale bars, 500 nm (H). (I) Quantitative analysis of mitochondrial cristae (the ratio of cristae number to mitochondrial area) in (H) (20–30 mitochondria per group, biological replicates).

Data information: Data are from three independent experiments (D) or at least three biological replicates (E–I) and presented as mean ± s.e.m. ns, not significant (*P* > 0.05), *P < 0.05, **P < 0.01, ***P < 0.001, using a two-tailed, unpaired Student's *t*-test.

Source data are available online for this figure.
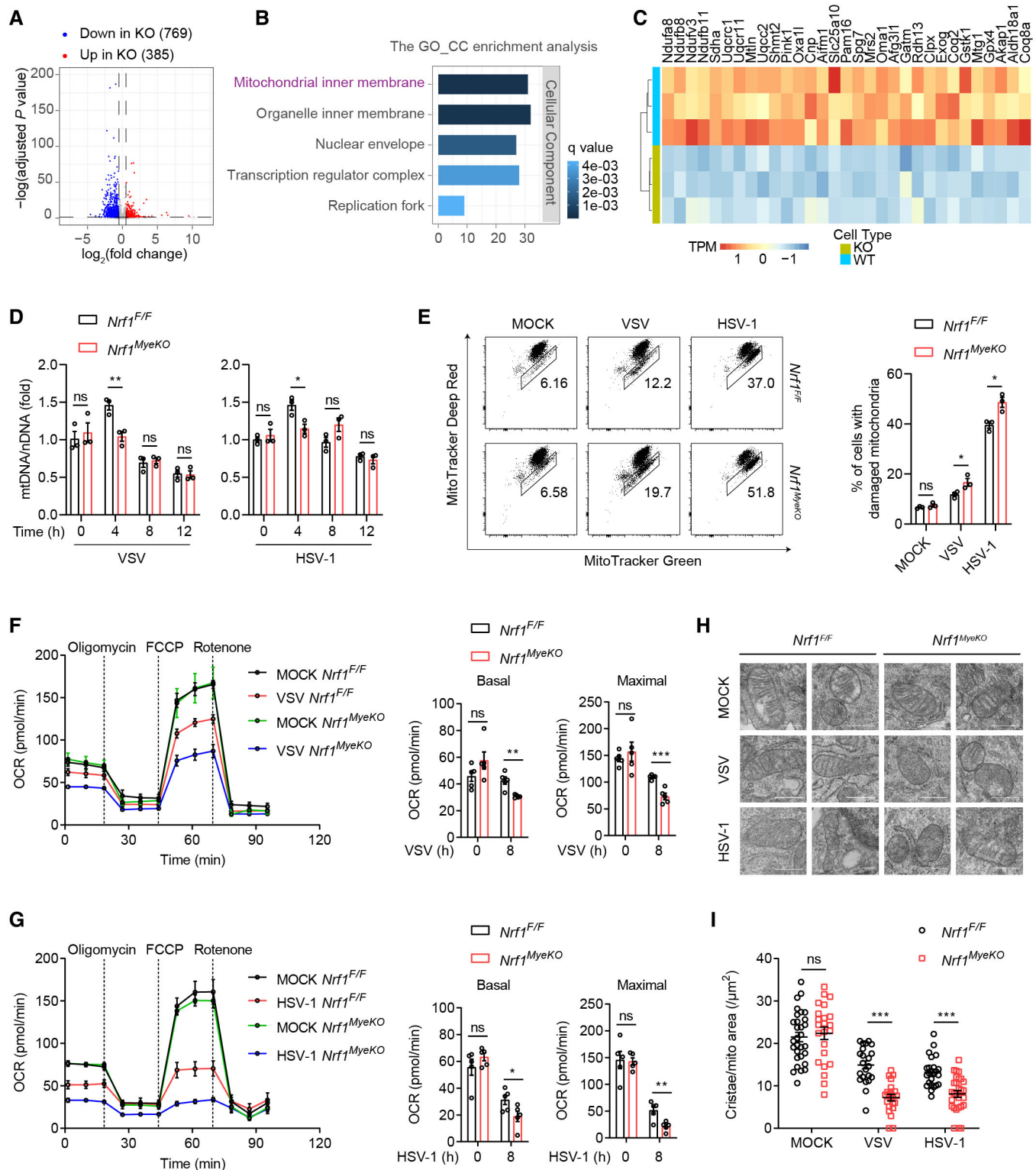
Figure 2.

Appendix Fig S3), which is consistent with the report that loss of an individual accessory subunit often disrupted assembly of complex I (Stroud et al, 2016). Furthermore, although a decreased level of mtDNA was observed in NRF1-knockdown PMs, the mitochondrial mass determined by mtDNA/nDNA ratio showed no significant difference between wild-type and NRF1-KO PMs (Fig EV2C). We reason that the long-term ablation of NRF1 may activate some compensatory effects to prevent mtDNA depletion in

NRF1-KO PMs. Notably, *Tfam*, a canonical NRF1 target gene whose major function is to regulate mtDNA replication and transcription, was downregulated by NRF1 deficiency at 8-h postinfection with VSV or HSV-1 but not at steady state (Fig EV2D). These data suggest that NRF1 may only function in mitochondrial quality control during viral infection.

We next tested the effect of NRF1 deficiency on mitochondrial quality upon viral infection. In NRF1-KO PMs, virus-induced expression of mitochondrial proteins (NDUFB8, SDHA, UQCRC1) was significantly blocked (Fig EV2E and F). Consistently, the increase of mtDNA copy number at 4-h postinfection with VSV or HSV-1 was also blocked in NRF1-KO PMs, which indicated that NRF1 deficiency inhibits mitochondrial biogenesis after viral infection (Fig 2D). However, differences in mtDNA copy number between wild-type and NRF1-KO PMs were disappeared at the late phase of viral infection (8 and 12 h) (Fig 2D), suggesting that NRF1 deficiency may also affect some other mitochondrial quality control pathways. A previous study reported that NRF1 promotes mitophagy through the PINK1-Parkin mechanism. Postulating that NRF1-mediated synthesis of new mitochondria is the fundament for the subsequent elimination of damaged mitochondria via mitophagy, we next examined the effect of NRF1 deficiency on virus-induced mitophagy. We observed induced colocalization of mitochondria with endogenous LC3 after viral infection, which is significantly inhibited by NRF1 deficiency (Fig EV2G and H). To confirm that mitophagy flux was altered in NRF1-KO PMs, we co-stained for mitochondria and lysosomes using LysoTracker and found a decrease in colocalization of mitochondria with lysosomes in NRF1-KO PMs after viral infection (Fig EV2I and J), indicating that NRF1 deficiency attenuates virus-induced mitophagy.

Given that the loss of NRF1 inhibits mitochondrial biogenesis and mitophagy, we further investigated whether NRF1 deficiency triggers mitochondrial dysfunction. Using a fluorescence-based assay and flow cytometry to quantitate mitochondrial damage, we found that viral infection induced the appearance of damaged mitochondria, and this was exacerbated in NRF1-KO PMs (Fig 2E). To confirm these findings, we assessed the rates of mitochondrial oxidative phosphorylation (OxPhos) by measuring cellular oxygen consumption rate (OCR). The data suggested that NRF1-KO PMs exhibited a lower level of basal and maximal OxPhos compared with wild-type PMs after viral infection (Fig 2F and G). Transmission electron microscopy (TEM) analysis revealed that mitochondrial cristae appeared normal in wild-type and NRF1-KO PMs at baseline. By contrast, after viral infection, NRF1-KO PMs showed a stronger reduction of mitochondrial cristae compared with wild-type PMs (Fig 2H and I), indicating that NRF1 deficiency aggravates virus-induced mitochondrial damage. Taken together, our results suggest that NRF1-mediated mitochondrial quality control is critical for maintaining mitochondrial homeostasis during viral infection.

Of note, although the copy number of mtDNA was not changed in NRF1-KO PMs at steady state, we found that the cytosolic mtDNA was remarkably higher caused by NRF1 deficiency (**Appendix Fig S4A and B**). We speculated that NRF1 deficiency might promote the opening of mitochondrial permeability transition pore (MPTP) by affecting some mitochondrial inner membrane proteins and thus enhanced the release of mtDNA. To test this hypothesis, we blocked the opening of mPTP by cyclosporin A (CsA) and found that the effect of NRF1 deficiency on mtDNA release was significantly

inhibited (**Appendix Fig S4C**). Elevated cytosolic mtDNA often primes innate immune response in macrophages. To determine the activation of innate immunity in NRF1-KO PMs, we analyzed the total and phosphorylated levels of TBK1, p65, and STAT1, which are the central components in the NF-κB and type I interferon signaling pathways (Hayden & Ghosh, 2008; Takeuchi & Akira, 2010). The results showed that NRF1 deficiency had a limited effect on the total levels of TBK1, p65, and STAT1. However, the levels of phosphorylated TBK1, p65, and STAT1 were markedly increased in NRF1-KO PMs (**Appendix Fig S4D**). We also found that NRF1 deficiency induced mRNA expression of genes encoding type I IFN (*Ifna4*) or proinflammatory cytokines (*Il1b*), as well as transcription factors *Irf7*, interferon-stimulated genes (*Usp18*, *Mx1*, *Ifit1*, and *Ifit3*) that function to positively reinforce innate immune response (**Appendix Fig S4E**), implying that loss of NRF1 may achieve a great positive impact on innate antiviral response.

NRF1 negatively regulates innate antiviral signaling

To further explore the function of NRF1 in innate antiviral signaling, we performed luciferase reporter assays and found that overexpression of NRF1 attenuated VSV-induced activation of interferon-stimulated response element (ISRE), NF-κB and IFN-β promoter in a dose-dependent manner (Fig 3A). Overexpression of NRF1 also resulted in diminished expression of *IFNB1* induced by VSV or poly (I:C) in HEK293T cells (Fig EV3A). Conversely, using siRNA to silence NRF1, we found that poly(I:C)- and ISD-induced activation of TBK1, p65, and STAT1 was markedly increased in NRF1-knockdown PMs (Fig EV3B). Moreover, knockdown of NRF1 by siRNA substantially potentiated the expression of genes encoding type I interferon (*Ifnb1*) and proinflammatory cytokines (*Il6* and *Tnfa*) after infection with VSV or HSV-1 or stimulation with poly(I: C) or ISD (Fig EV3C–F). Consistently, qRT–PCR assay and plaque assay showed that the replication of virus was strongly inhibited by NRF1 depletion. (Fig EV3G and H).

We next infected wild-type and NRF1-KO PMs with VSV or HSV-1 and found that virus-induced phosphorylation of TBK1, p65, and STAT1 was remarkably enhanced in NRF1-KO PMs (Fig 3B). Similar results were obtained from mouse PMs stimulated with poly(I:C) or ISD (Fig 3C). Consistently, qRT–PCR analysis showed that the mRNA levels of *Ifnb1*, *Il6*, *Tnfa*, and *Cxcl10* were significantly increased in NRF1-KO PMs compared with wild-type PMs after infection with VSV or HSV-1, or stimulation with poly(I:C) or ISD (Fig 3D). Of note, the effects of NRF1-KO on the antiviral responses induced by these stimuli were not identical, which may be caused by their different signaling cascades. We next performed ELISA assay and found that the secretion of IFN-β, IL6, and TNF-α from NRF1-KO PMs was also much more abundant than that of wild-type PMs after treatment with various stimuli to activate innate antiviral immunity (Fig 3E). Such an elevated innate antiviral response coincided with a lower viral titer in NRF1-KO PMs (Fig 3F). Collectively, these results suggest a negative regulatory role of NRF1 in innate antiviral signaling.

NRF1 deficiency protects mice against viral infection

To elucidate the physiological role of NRF1 in host defense against viral infection *in vivo*, we challenged *Nrf1^MyeKO^* (NRF1-KO) mice and their *Nrf1^F/F^* (wild-type) littermates with VSV or HSV-1. IFN-β,

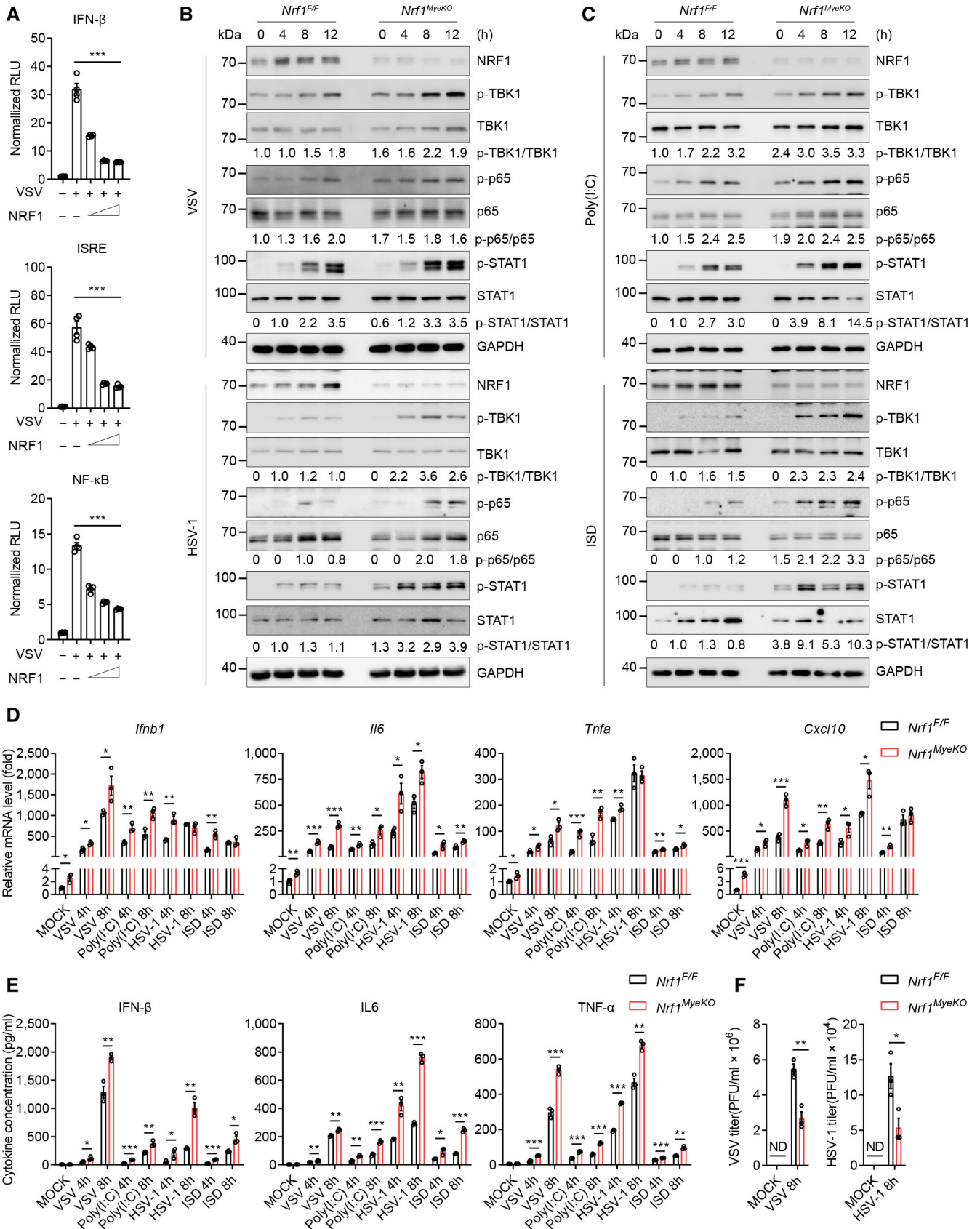**Figure 3.**

◀

Figure 3. NRF1 negatively regulates innate antiviral signaling.

A   Luciferase activity of IFN-β, NF-κB, and ISRE promoter reporter in HEK293T cells transfected with empty vector or plasmids encoding incremental NRF1-Myc for 24 h followed by infection with VSV for 8 h (*n* = 4 biological replicates per group).

B, C   Immunoblot analysis of phosphorylated and total TBK1, p65, and STAT1 in wild-type and NRF1-KO mouse PMs infected with VSV or HSV-1 (B) or stimulated with poly(I:C) or ISD (C) for the indicated time points. GAPDH was used as a loading control. Ratios of phosphorylated proteins versus total proteins normalized to the 0- or 4-h time point of each wild-type sample.

D   qPCR analysis of *Ifnb1*, *Il6*, *Tnfa* and *Cxcl10* mRNA in wild-type and NRF1-KO mouse PMs infected with VSV or HSV-1 or stimulated with poly(I:C) or ISD for the indicated time points (*n* = 3 biological replicates per group).

E   ELISA quantification of IFN-β, IL6, and TNF-α secretion in wild-type and NRF1-KO mouse PMs treated as in (D) (*n* = 3 biological replicates per group).

F   Plaque assay of VSV and HSV-1 titers in wild-type and NRF1-KO mouse PMs at 8 h after infection with those viruses (*n* = 3 biological replicates per group).

Data information: Data are from three independent experiments (D–F) or representative data (B and C) and presented as mean ± s.e.m. ND, not detectable, *$P < 0.05$, **$P < 0.01$, ***$P < 0.001$, using a two-tailed, unpaired Student's *t*-test.

Source data are available online for this figure.

IL6, and TNF-α protein abundance in the sera after VSV or HSV-1 infection was significantly increased in the NRF1-KO mice compared with those in the wild-type littermates (Fig 4A). For VSV infection, the results showed that the expression of *Ifnb1*, *Il6*, and *Tnfa* were significantly higher in the lungs of NRF1-KO mice than in the lungs of wild-type littermates at 24 h after infection (Fig 4B), whereas the replication of VSV in the lungs of NRF1-KO mice was severely compromised compared with the wild-type littermates (Fig 4C). Hematoxylin and eosin (HE) staining also showed less injury in the lungs of NRF1-KO mice after VSV infection (Fig 4D). During HSV-1 infection, the hyperactivation of innate antiviral response was also observed in the brain tissues of NRF1-KO mice (Fig 4E). In addition, the mRNA levels of HSV-1 *UL30* gene and HSV-1 viral titers were significantly decreased in the brains of NRF1-KO mice compared with the brains of wild-type littermates (Fig 4F). We next infected NRF1-KO mice and wild-type littermates by intraperitoneal infection of HSV-1 and monitored their survival. The results showed that NRF1-KO mice possessed lower mortality than wild-type mice upon infection with HSV-1 (Fig 4G). Collectively, these results suggest that NRF1 deficiency enhanced resistance to viral infection *in vivo*.

Mitochondrial DAMPs promoted by NRF1 deficiency contribute to the innate antiviral immunity

Next, we sought to examine how NRF1 deficiency promotes innate antiviral immunity. MtROS and mtDNA are two main mitochondrial DAMPs that have important roles in the control of viral survival and innate antiviral response in macrophages (Zhou *et al*, 2011; Elliott & Sutterwala, 2015), and accumulation of damaged mitochondria often correlates with higher mtROS production and elevated mtDNA release (Nakahira *et al*, 2011; Palikaras *et al*, 2018). We therefore checked whether the enhanced innate antiviral response in NRF1-KO macrophages was due to aberrant mtROS production and mtDNA release. Using the mitochondria-specific ROS indicator MitoSOX, we first confirmed that VSV or HSV-1 induced a significant increase in the level of mtROS in mouse PMs at 12 h after infection with VSV or HSV-1, or stimulation with poly(I:C) or ISD (Fig EV4A). On the other hand, mtDNA release was readily apparent after 4 h of HSV-1 challenge or ISD stimulation, whereas VSV infection or poly(I:C) stimulation could not induce mtDNA stress (Fig EV4B).

Given that the infection of virus induces the release of mitochondrial DAMPs, we wanted to know whether NRF1 deficiency promotes these processes. In NRF1-KO PMs, we found that VSV and HSV-1 induced an enhancement of mtROS production as early as 4 h

after infection, which is not appeared in wild-type PMs (Fig 5A). Notably, NRF1 deficiency led to a lower level of basal mtROS, which may be caused by the reduction of respiratory complex I, a main site at which electrons leak to oxygen and result in superoxide production. To investigate whether NRF1 deficiency had an effect on mtDNA release upon viral infection, we isolated pure cytosolic fractions from VSV or HSV-1-infected wild-type and NRF1-KO PMs and quantified the mtDNA amount via qPCR. We detected significant enrichment for mtDNA (*mt-Rnr2* and *mt-Nd4*) in the cytosolic compartments of NRF1-KO PMs when compared to wild-type PMs (Fig 5B). Using an anti-DNA antibody to indicate DNA, we found that NRF1 deficiency decreased the colocalization between mtDNA and mitochondria in PMs (Fig 5C and D). These results indicate that NRF1 deficiency promotes mitochondrial DAMPs production during viral infection.

We further determined whether the elimination of mitochondria-derived DAMPs would reverse the enhanced innate antiviral response in NRF1-KO PMs. Through treating mouse PMs with ethidium bromide (EtBr), a mtDNA replication inhibitor, which depletes mtDNA and blocks mitochondrial function (Zhong *et al*, 2016), we found that mtDNA depletion inhibited the activation of innate antiviral response and attenuated excessive IL6 and IFN-β secretion in both wild-type and NRF1-KO PMs after viral infection (Figs 5E and EV4C and D). Next, we examined whether sequestering mtROS would attenuate the effect of NRF1 deficiency. Using a mtROS scavenger (MitoQ) (Chernyak *et al*, 2006), we found that virus-induced higher activation of *Ifnb1* and *Il6* resulting from NRF1 deficiency was lost after the treatment of MitoQ (Figs 5F and EV4E). We further confirmed that mitochondrial DAMPs also contributed to poly (I:C)- and ISD-induced innate antiviral immunity in NRF1-KO PMs (**Appendix Fig S5A and B**). Moreover, we challenged *Nrf1^MyeKO* (NRF1-KO) mice and their *Nrf1^{F/F}* (wild-type) littermates with VSV or HSV-1 and found that virus-induced enhanced innate antiviral response in NRF1-KO mice was reversed by MitoQ pretreatment (Figs 5G–I and EV4F). These data collectively suggest that deficiency of NRF1-mediated mitochondrial quality control potentiates virus-induced mitochondrial DAMPs release and thereby enhancing innate antiviral immunity.

Ser318 of NRF1 is critical for the innate antiviral response during HSV-1 infection

Although both VSV and HSV-1 promoted mitochondrial DAMPs production, we note that only HSV-1 could induce mtDNA release in
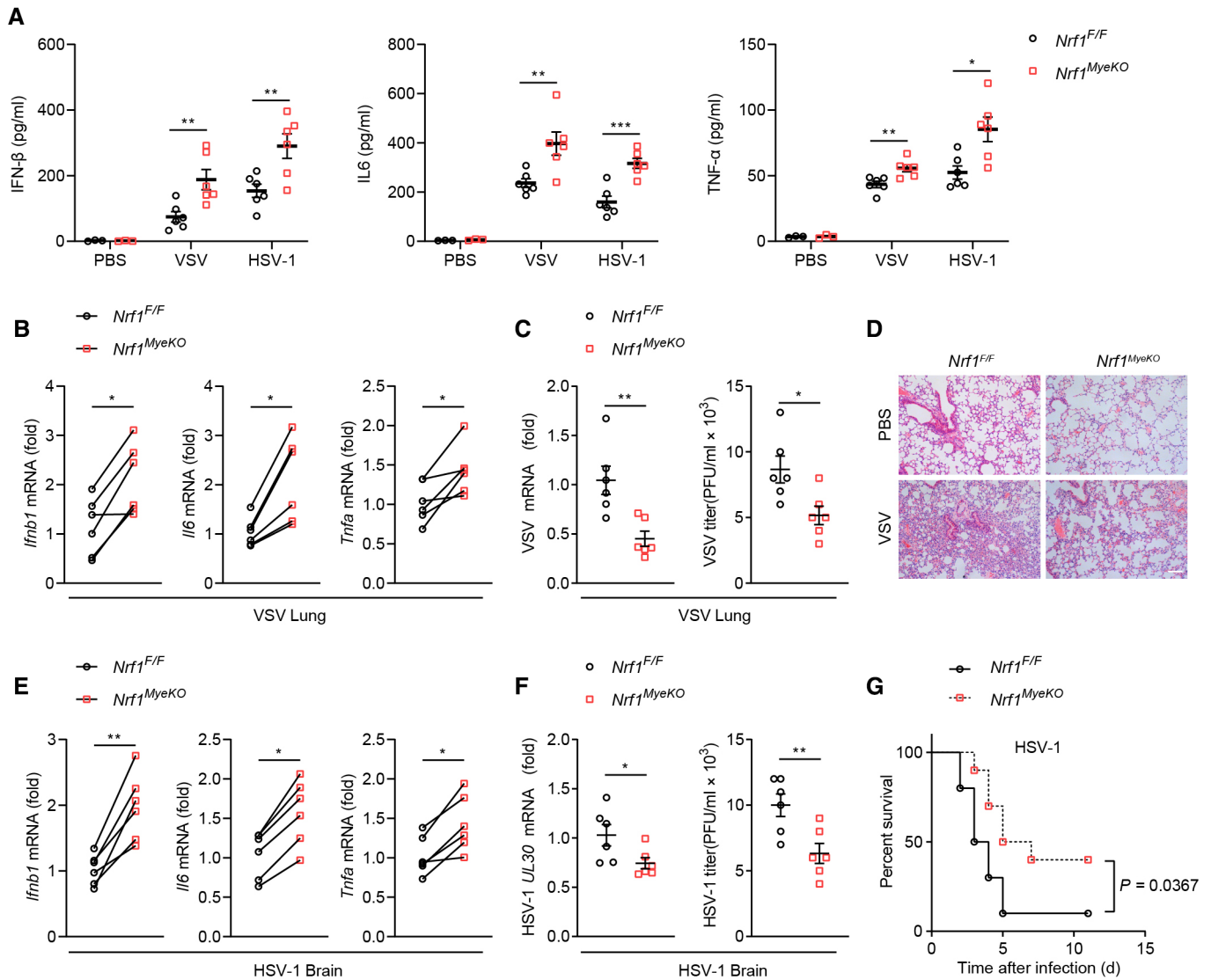
Figure 4. NRF1 deficiency protects mice against viral infection.

A 8-week-old *Nrf1^{F/F}* and *Nrf1^{MyeKO}* mice ($n = 3$ for PBS treatment and $n = 6$ for virus treatment) were intravenously infected with VSV (4×10^7 PFU/mouse) or HSV-1 (1×10^7 PFU/mouse). After 24 h, ELISA quantification of IFN-β, IL6, and TNF-α in sera.

B qPCR analysis of *Ifnb1*, *Il6*, and *Tnfa* mRNA in the lung of *Nrf1^{F/F}* and *Nrf1^{MyeKO}* mice infected with VSV as in A ($n = 6$ per group).

C qPCR analysis of VSV mRNA and plaque assay of VSV titers in the lungs of *Nrf1^{F/F}* and *Nrf1^{MyeKO}* mice infected with VSV as in A ($n = 6$ per group).

D Hematoxylin–eosin staining of lung sections from mice treated with PBS or VSV as in (A). Scale bar, 100 μm.

E qPCR analysis of *Ifnb1*, *Il6*, and *Tnfa* mRNA in the brains of *Nrf1^{F/F}* and *Nrf1^{MyeKO}* mice infected with HSV-1 as in (A) ($n = 6$ per group).

F qPCR analysis of HSV-1 *UL30* mRNA and plaque assay of HSV-1 titers in the brain of *Nrf1^{F/F}* and *Nrf1^{MyeKO}* mice infected with HSV-1 as in (A) ($n = 6$ per group).

G Survival of *Nrf1^{F/F}* and *Nrf1^{MyeKO}* mice ($n = 10$ per group) at various times after intraperitoneal (i.p.) infection with HSV-1 (2×10^7 PFU per mouse).

Data information: Data are presented as mean ± s.e.m. The two-tailed, unpaired Student's *t*-test (A–F) or log-rank (Mantel–Cox) test (G) were used to measure significance. *$P < 0.05$, **$P < 0.01$, ***$P < 0.001$.
Source data are available online for this figure.

wild-type and NRF1-KO PMs as early as 4 h after infection. We speculated that HSV-1 might control NRF1 activity in an unrecognized manner. It has been shown that the activity of NRF1 was highly correlated with its phosphorylation level (Gugneja & Scarpulla, 1997; Chow *et al*, 2019; Palmer *et al*, 2019). To determine whether NRF1 was phosphorylated during viral infection, we performed Phos-tag mobility shift assay (PTMSA) and found that HSV-1 infection, but

not VSV infection, induced a significant migration of NRF1 band, which indicated an increased phosphorylation level of NRF1 after the infection of HSV-1 (Fig 6A). We next explored which kinase was responsible for NRF1 phosphorylation. TBK1 was an important serine/threonine kinase in the innate immune system. A shifting band often accompanied substrate phosphorylation induced by TBK1 in PTMSA and SDS–PAGE (Heo *et al*, 2015, 2018; Zhao *et al*, 2018).
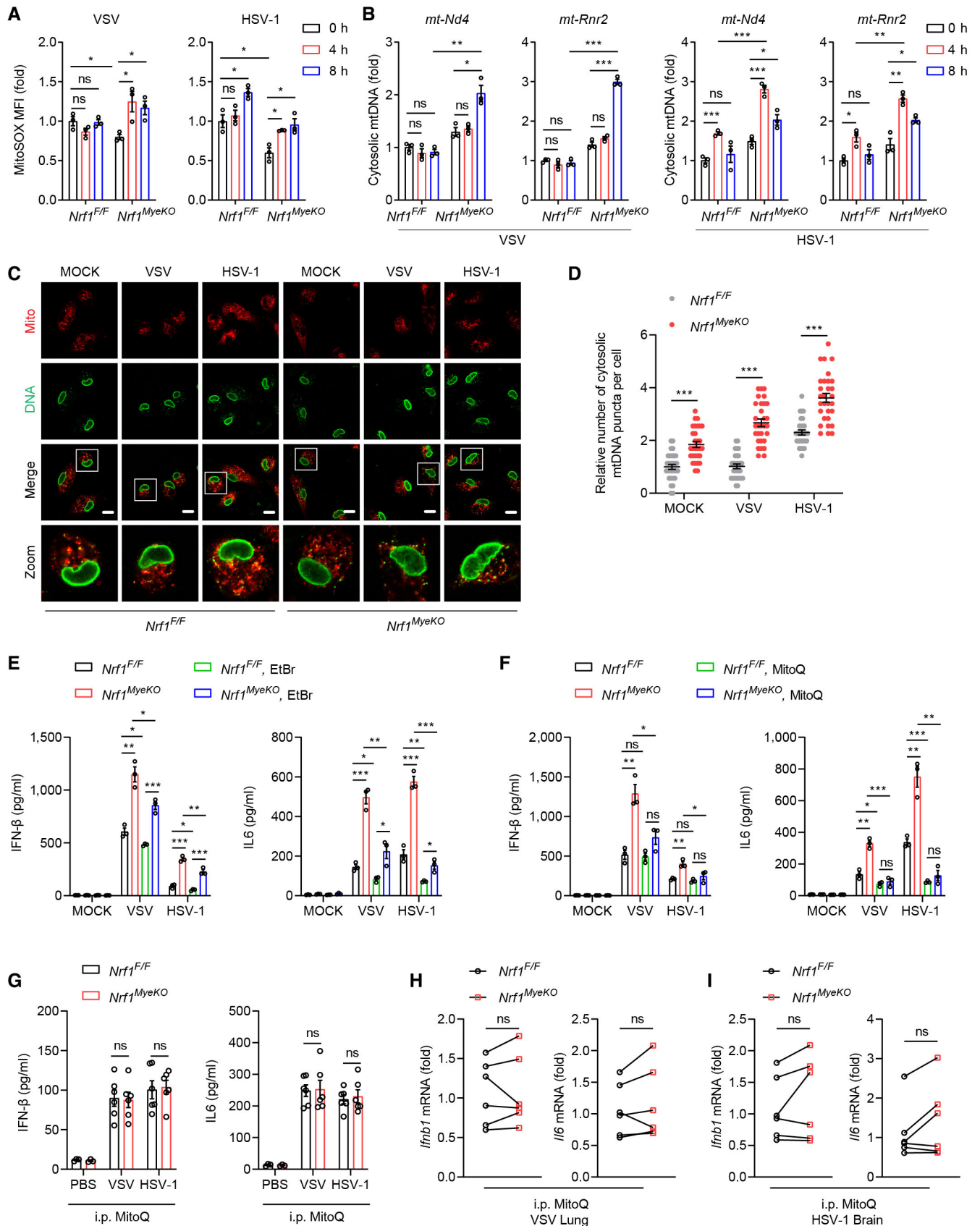
Figure 5.

Figure 5.   Mitochondrial DAMPs promoted by NRF1 deficiency contribute to the innate antiviral immunity.

A   mtROS levels measured by MitoSOX staining and flow cytometry in wild-type and NRF1-KO mouse PMs infected with VSV (left) or HSV-1 (right) for the indicated time points. MFI, mean fluorescence intensity ($n = 3$ biological replicates per group).

B   DNA was isolated from digitonin extracts of wild-type and NRF1-KO mouse PMs infected with VSV (left) or HSV-1 (right) for the indicated time points. Cytosolic translocation of mtDNA was quantified via qPCR using the indicated primer sets. *18S rRNA* served as a control ($n = 3$ biological replicates per group).

C, D   Wild-type and NRF1-KO mouse PMs infected with VSV (8 h) or HSV-1 (4 h) were imaged by confocal microscope after staining with anti-DNA (DNA) and anti-Prohibitin (Mito) antibodies. Scale bars, 5 μm (C). (D) The number of cytosolic mtDNA puncta per cell was quantitated by ImageJ ($n = 30$ cells per group).

E   ELISA quantification of IFN-β (left) and IL6 (right) in wild-type and NRF1-KO mouse PMs pretreated with or without EtBr (450 ng/ml, 72 h), followed by infection with VSV or HSV-1 for 8 h ($n = 3$ biological replicates per group).

F   ELISA quantification of IFN-β (left) and IL6 (right) in wild-type and NRF1-KO mouse PMs pretreated with or without MitoQ (100 nM, 2 h), followed by infection with VSV or HSV-1 for 8 h ($n = 3$ biological replicates per group).

G   ELISA quantification of IFN-β (left) and IL6 (right) from *Nrf1^{F/F}* and *Nrf1^{MyeKO}* mice pretreated with MitoQ (5 mg/kg body weight, i.p. injection) for 1 h and then infected i.p. with PBS, VSV (5×10^8 PFU/mouse) or HSV-1 (1×10^7 PFU/mouse) for 24 h ($n = 3$ for PBS treatment and $n = 6$ for virus treatment).

H   qPCR analysis of *Ifnb1* and *Il6* mRNA in the lungs of *Nrf1^{F/F}* and *Nrf1^{MyeKO}* mice pretreated with MitoQ as in (G) and 1 h later infected i.p. with VSV (5×10^8 PFU/mouse) for 24 h ($n = 6$ per group).

I   qPCR analysis of *Ifnb1* and *Il6* mRNA in the brains of *Nrf1^{F/F}* and *Nrf1^{MyeKO}* mice pretreated with MitoQ as in (G) and 1 h later infected i.p. with HSV-1 (1×10^7 PFU/mouse) for 24 h ($n = 6$ per group).

Data information: Data are from three independent experiments (A, B, and D–F) or representative data (C) and presented as mean ± s.e.m. ns, not significant ($P > 0.05$), *$P < 0.05$, **$P < 0.01$, ***$P < 0.001$, using a two-tailed, unpaired Student's *t*-test.
Source data are available online for this figure.

We found that overexpression of TBK1 wild-type (WT) but not TBK1 K38A kinase-dead mutant (KD) resulted in a shift of NRF1 band in SDS–PAGE (Figs 6B and EV5A). Calf-intestinal alkaline phosphatase (CIP) treatment of cell lysates abolished the shift induced by wild-type TBK1 (Fig EV5B). We further found that NRF1 strongly interacted with TBK1 and this association was enhanced during HSV-1 infection (Fig 6C and D). *In vitro* kinase assay also showed increased phosphorylation of NRF1 induced by wild-type TBK1 but not kinase-dead TBK1 (Fig 6E). These data indicated that TBK1 could interact with and phosphorylate NRF1.

To further address the phosphorylated sites in NRF1 by TBK1, NRF1 immunoprecipitated from HEK293T cells with wild-type TBK1 or kinase-dead TBK1 overexpression was detected by antibody targeting phospho-Ser or phosphor-Thr, respectively. The results showed that the mobility shift of NRF1 could only be recognized by phospho-Ser antibody indicating that NRF1 is phosphorylated by

TBK1 on serine residues (Fig EV5C). We next constructed different NRF1 truncations and identified the amino acids 301–503 on NRF1 as the phosphorylated region by TBK1 (Fig EV5D). We subsequently constructed a series of NRF1 point mutants and found that Ser318 and Ser384 were two critical residues for the mobility shift of NRF1 induced by TBK1 (Fig EV5E). Although the Ser393 of NRF1 also mediated a shifting band of NRF1, it has no effect on TBK1-induced NRF1 mobility shift. Notably, the point substitution 2SA (S318A/S384A) almost completely blocked the phosphorylated shift of NRF1 induced by TBK1 (Fig EV5F and G). A comparison of NRF1 sequences from multiple species revealed that both Ser318 and Ser384 are conserved (Fig EV5H). Furthermore, utilizing an antibody specific for the NRF1 Ser318-phosphorylation site, we detected robust signal for NRF1 phosphorylated at Ser318 induced by TBK1 (Figs 6F and EV5I). We then investigated the potential effect of TBK1-mediated phosphorylation on the transcriptional activity of

Figure 6.   Ser318 of NRF1 is critical for the innate antiviral response during HSV-1 infection.

A   Immunoblot analysis and Phos-tag SDS–PAGE analysis of mouse PMs infected with VSV or HSV-1 for the indicated time points.

B   Immunoblot analysis of whole-cell lysates from HEK293T cells transfected to express Flag-TBK1 WT or Flag-TBK1 kinase-dead mutant (KD).

C   Interaction between TBK1 and NRF1 in HEK293T cells was detected by co-immunoprecipitation of differentially tagged proteins.

D   The endogenous complex of TBK1 and NRF1 in iBMDM cells was revealed by co-immunoprecipitation using anti-TBK1 antibody and visualized by using anti-NRF1 antibody.

E   HEK293T cells were transfected to express Flag-TBK1 WT or Flag-TBK1 kinase-dead mutant (KD) for 24 h and harvested. The immunoprecipitated Flag-TBK1 WT or Flag-TBK1 KD was incubated with purified His-NRF1 in the presence of unlabeled ATP and resolved by SDS–PAGE, followed by immunoblot analysis with antibody to phospho-Ser/Thr, anti-NRF1 or anti-Flag.

F   HEK293T cells were transfected to express NRF1-Myc WT or NRF1-Myc S318A with Flag-TBK1 WT or Flag-TBK1 kinase-dead mutant (KD) for 24 h and harvested. The cell lysates were immunoprecipitated with anti-Myc antibody, followed by immunoblot analysis with antibody to NRF1 phosphorylated at Ser318, anti-Myc, or anti-Flag.

G   Endogenous phospho-NRF1 S318 signal was detected in wild-type and NRF1 S318A mouse PMs after the infection with different viruses for 8 h. The red arrows indicate phosphorylated signals for NRF1.

H   Heatmap showing the relative expression of mitochondrial genes in wild-type and NRF1 S318A mouse PMs at steady state and 8 h after infection with HSV-1. Expression signals are depicted using pseudocoloring, in which expression for each gene is shown as high (red) or low (blue) ($n = 3$ biological replicates per group).

I   qPCR analysis of *Ifnb1* and *Il6* mRNA in wild-type and NRF1 S318A mouse PMs infected with VSV or HSV-1 for 8 h ($n = 3$ biological replicates per group).

J   ELISA quantification of IFN-β and IL6 secretion in wild-type and NRF1 S318A mouse PMs treated as in (I) ($n = 3$ biological replicates per group).

K   8-week-old wild-type and NRF1 S318A mice ($n = 3$ for PBS treatment and $n = 6$ for HSV-1 treatment) were intravenously infected with HSV-1 (1×10^7 PFU/mouse). After 24 h, ELISA quantification of IFN-β, IL6, and TNF-α in sera.

L   Survival of wild-type and NRF1 S318A mice ($n = 10$ per group) at various times after intraperitoneal infection with HSV-1 (2×10^7 PFU per mouse).

Data information: Data are from three independent experiments (H–J) or representative data (A-G) and presented as mean ± s.e.m. ns, not significant ($P > 0.05$), *$P < 0.05$, **$P < 0.01$. The two-tailed, unpaired Student's *t*-test (I–K) or log-rank (Mantel–Cox) test (L) were used to measure significance.
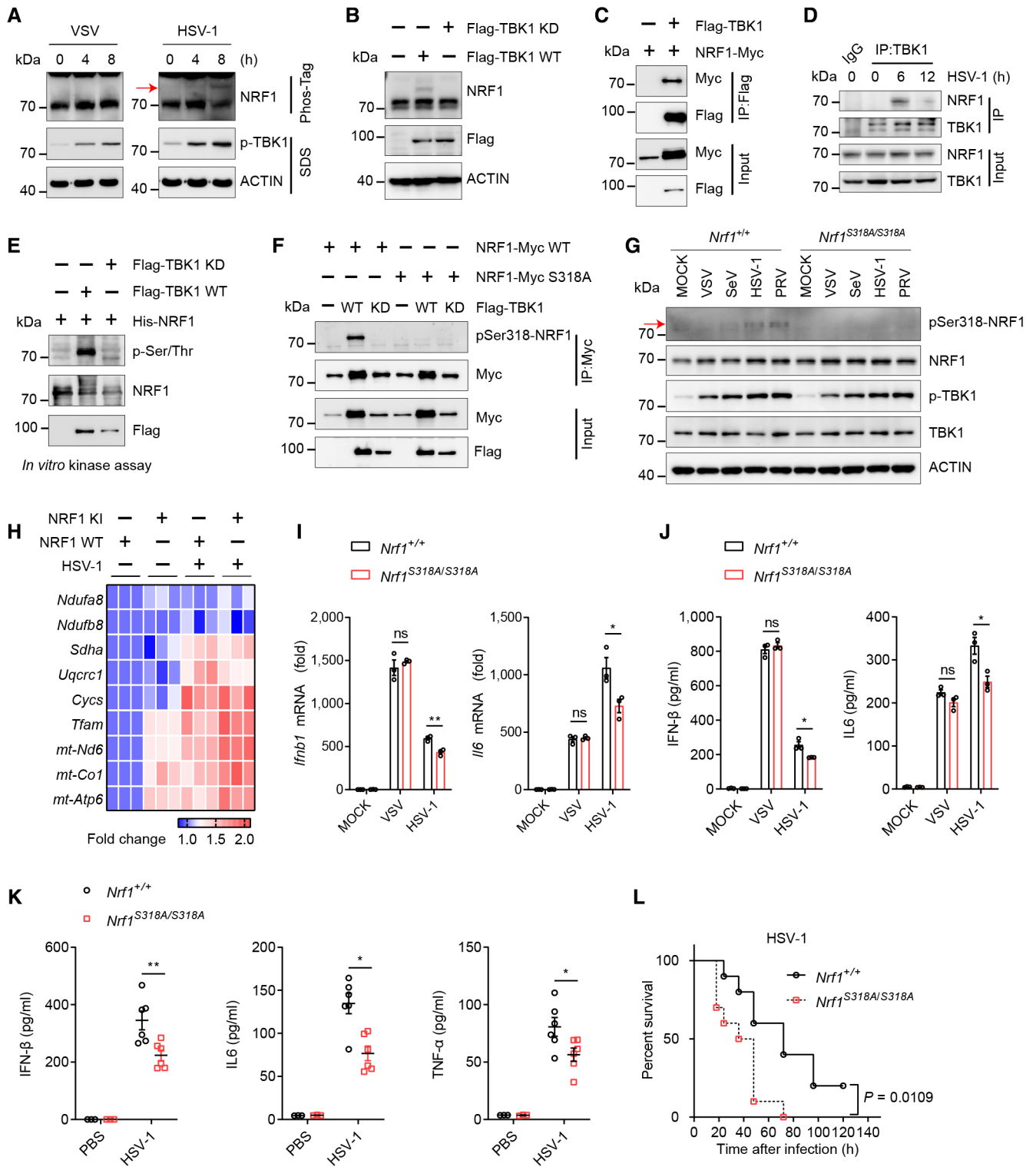Source data are available online for this figure.

Figure 6.

NRF1. We indeed observed that the phosphorylation-defective S318A, S384A, and 2SA NRF1 mutants induced a significant increase in NRF1-driven *TFAM* luciferase reporter activation compared with their phosphorylation-mimicking S318D, S384D, and 2SD NRF1 mutants, respectively (**Appendix Fig S6A**). Consistently,

an electrophoretic mobility shift assay (EMSA) analysis showed that the S318A and S384A NRF1 mutants exhibited a higher binding activity to NBE-probe (a synthesized DNA containing NRF1 binding sites in *TFAM* promoter region, NRF1 binding element) than their S318D and S384D NRF1 mutants, respectively (**Appendix Fig S6B**).

These data suggest that TBK1 phosphorylates and inactivates NRF1 during HSV-1 infection.

To further understand the functional importance of TBK1-induced phosphorylation of NRF1, we generated knock-in (KI) mice by CRISPR-based genome editing to mutate NRF1 residue Ser318 into alanine. Homozygous mutant mice were viable and fertile and showed no obvious difference in sizes and morphologies compared with wild-type mice (**Appendix Fig S6C**). We next test whether the phosphorylation of NRF1 at Ser318 induced by TBK1 is unique to DNA virus. We used another RNA virus, Sendai Virus (SeV), and another DNA virus, Pseudorabies Virus (PRV), and found that the DNA virus HSV-1 and PRV could induce a significant increase in the phosphorylated level of NRF1 at Ser318 in wild-type PMs but not in NRF1 S318A PMs (Fig 6G). However, a slight signal for NRF1 phosphorylated at Ser318 was detected after the infection of SeV but not VSV, which indicated that the phosphorylation of NRF1 is subject to multiple regulatory mechanisms during RNA virus infection. Given that the phosphorylation at Ser318 had an impact on the transcriptional activity of NRF1, we next sought to examine how NRF1 S318A mutation affects mitochondrial quality upon HSV-1 infection. Results from qRT–PCR analysis suggested that wild-type and NRF1 S318A PMs exhibited no significant difference in the transcript levels of many NEMGs (*Ndufa8*, *Ndufb8*, *Sdha*, *Uqcrc1*, *Cycs*) at steady state and 8-h postinfection with HSV-1. Interestingly, the transcription of *Tfam* and mtDNA was markedly enhanced in NRF1 S318A PMs (Fig 6H). Consistent with the increased mRNA levels of *Tfam* and mtDNA-encoded genes, the protein levels of TFAM and mtDNA-encoded mitochondrial respiratory complexes subunits, such as cytochrome *c* oxidase subunit 2 (mt-CO2) and mitochondrial-encoded ATP synthase membrane subunit 6 (mt-ATP6), were remarkably higher in NRF1 S318A PMs than those in wild-type PMs (**Appendix Fig S6D**).

Next, we determined whether NRF1 S318A mutation affects innate antiviral immunity. Previous studies have shown that TFAM depletion impairs mtDNA transcription and induces mtDNA release, which subsequently activates cGAS-STING and NF-κB signaling (West *et al*, 2015; Chung *et al*, 2019). Analysis of isolated pure cytosolic extracts revealed that the cytosolic mtDNA was remarkably reduced in NRF1 S318A PMs compared with wild-type PMs at steady state and 4-h postinfection with HSV-1 (**Appendix Fig S6E**). Consistently, HSV-1 but not VSV induced a significantly lower activation of *Ifnb1* and *Il6* in NRF1 S318A PMs (Fig 6I and J). Furthermore, we challenged wild-type and NRF1 S318A KI mice with HSV-1 and found that the protein level of IFN-β, IL6, and TNF-α in sera were significantly decreased in NRF1 S318A KI mice compared with those in wild-type mice (Fig 6K). In addition, NRF1 S318A KI mice showed higher mortality than wild-type mice after infection with HSV-1 (Fig 6L). Collectively, these data indicate that TBK1-induced NRF1 phosphorylation is critical in regulating mtDNA stress and physiologically important to host antiviral defense.

Discussion

The maintenance of host mitochondrial homeostasis is essential for the activation of innate immunity. Despite initiation that may be independent of mitochondria, numerous innate immune responses are still regulated by mitochondria as the transmission of their signals requires mitochondrial platform or components. Increasing data suggest that many innate immune signaling pathways are highly integrated with cellular mitochondrial quality control process, which not only remodels mitochondrial networks but also provides guidance for the survival of pathogens. For example, mitophagy and mitochondrial dynamics could be manipulated by pathogens to remove damaged mitochondria from the host and benefit viral or microbial survival (Li *et al*, 2005; Kim *et al*, 2014; Zhang *et al*, 2019). Several viruses could induce mitochondrial fission, which subsequently activates mitophagy during infection (Kim *et al*, 2013; Li *et al*, 2016).

However, whether and how mitochondrial biogenesis is regulated in response to infection is largely unknown. In this study, we identified and characterized a novel role of NRF1 in regulating innate antiviral immunity. Viral infection induced a NF-κB-dependent activation of NRF1-mediated mitochondrial biogenesis, which was reflected by increases in mitochondrial proteins, mitochondrial genes mRNA level, and mtDNA copy number. Abrogation of NRF1-mediated mitochondrial biogenesis significantly aggravated virus-induced mitochondrial damage and enhanced innate antiviral immunity in macrophages and mice (Fig 7). These findings revealed the importance of NRF1-mediated mitochondrial biogenesis in the control of overall mitochondria functionality and innate antiviral immunity.

Innate immunity plays a critical role in detecting and correcting both infectious and sterile insults. Activation of innate immune response requires the recognition of the insult through pattern recognition receptors (PRRs) (Takeuchi & Akira, 2010). These PRRs could bind to their specific activating ligands, including viral nucleic acids, endogenous DAMPs, and synthetic DNA or RNA, and trigger multiple signaling cascades that culminate in the activation of NF-κB, MAPK, and type I interferon pathways (Hayden *et al*, 2006; West *et al*, 2006; Takeuchi & Akira, 2009). In the present study, we demonstrated that various stimuli used to activate innate immunity could enhance the expression of NRF1 in a NF-κB-dependent manner. Although HSV-1 and ISD appeared to have a stronger effect on NRF1 expression compared with VSV and poly(I:C), which may be caused by the difference in the beginning and discrete steps of their signaling cascades, we did observe the activation of NRF1 targets after VSV and HSV-1 infection.

NRF1 has been identified as an important regulator of mitochondrial biogenesis through governing the expression of mitochondrial components (Virbasius & Scarpulla, 1994; Scarpulla *et al*, 2012). Activation of NRF1 often induces increased mitochondrial number accompanied by the augmentation of mitochondrial respiratory capacity. However, to maintain an optimal state of cellular mitochondrial quality, mitochondrial biogenesis was tightly coordinated with mitophagy (Palikaras & Tavernarakis, 2014; Liu *et al*, 2021a). The balance between these two opposing forces determines the mitochondrial turnover rate and maintains a healthy mitochondrial pool. In our study, an increased mitochondrial mass induced by NRF1 activation occurs at an early phase of viral infection, which is considered as the preparation for the subsequent elimination of damaged mitochondria via mitophagy. A previous study had also linked NRF1 to mitophagy through positive regulation of PINK1 and PARKIN (Lu *et al*, 2020). Here, a decreased mRNA level of *Pink1*
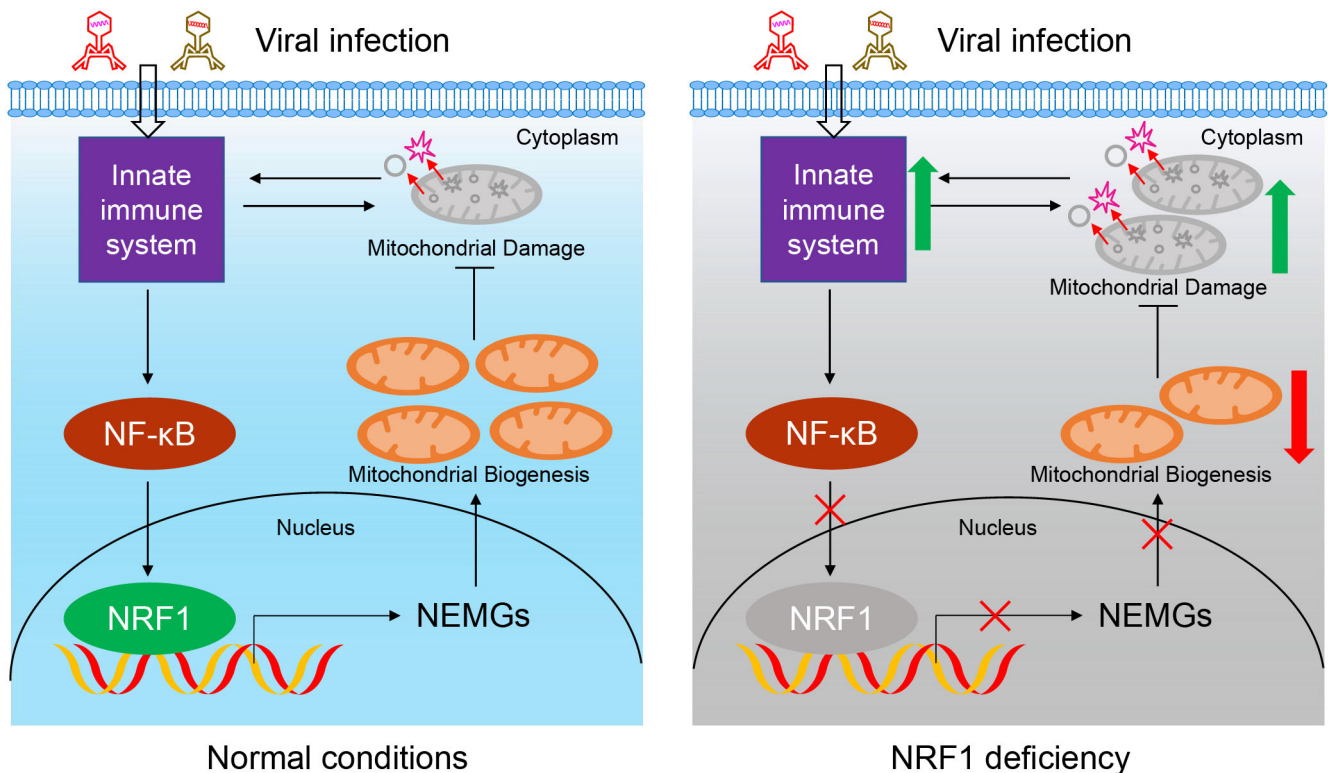
Figure 7. A proposed model of the NRF1-mediated mitochondrial biogenesis in regulating innate antiviral immunity.

was observed in NRF1-KO PMs, and virus-induced mitophagy was also partially inhibited by NRF1 deficiency. Given the importance of NRF1 to the balance of mitochondrial biogenesis and mitophagy, it is found that NRF1 deficiency significantly exacerbated virus-induced mitochondrial damage. The DAMPs derived from damaged mitochondria subsequently induced hyperactivation of innate anti-viral immunity in NRF1-KO PMs and mice. Some studies have suggested that a default in mitophagy leads to mitochondrial DAMPs release (Zhong *et al*, 2016; Li *et al*, 2019), which seems to attribute the effect of NRF1 deficiency on innate immunity to mitophagy. However, the regulatory function of NRF1 on mitophagy is associated with its transcriptional activation of mitochondrial genes, and NRF1-mediated mitochondrial biogenesis is initiated earlier than the occurrence of mitophagy, so we consider NRF1-mediated mitochondrial biogenesis as the primary contributor to the regulation of innate immunity.

Although we focused primarily on the mitochondrial homeostasis to demonstrate how NRF1 depletion affects host response to viral infection, it should not be inferred that the function of NRF1 is limited to the regulation of mitochondria in innate immune system. Genome-wide chromatin immunoprecipitation (ChIP) analyses have identified thousands of genes whose promoters are occupied by NRF1 in somatic cells (Satoh *et al*, 2013; Domcke *et al*, 2015), indicating the much broader function of NRF1 that have not been clarified. In our transcriptomic profile, NRF1 deficiency caused significant changes in various biological processes, including DNA repair, cell cycle, ncRNA metabolic process, and macromolecule methylation. Of note is that several of these processes also have an

association with innate immunity. DNA repair could respond to DNA damage and further regulate cGAS-STING pathway (Li & Chen, 2018; Guan *et al*, 2021; Liu *et al*, 2021b). Depletion of Ataxia-telangiectasia mutated (ATM), a central component of the DNA repair machinery, resulting in increased antiviral and antibacterial response in mice due to the aberrant accumulation of cytosolic DNA (Hartlova *et al*, 2015; Wang *et al*, 2020). Furthermore, previous studies provided evidence that the methylation of DNA, RNA, or proteins is important for regulating innate immunity (Zhang & Cao, 2019; Beck *et al*, 2021; Xu *et al*, 2021; Zhu *et al*, 2021). Therefore, it is conceivable that NRF1 modulates the expression of multiple genes and controls different biological processes in macrophages simultaneously.

We also identified that TBK1 could phosphorylate NRF1 during HSV-1 infection. Direct phosphorylation of two NRF1 residues by TBK1, Ser318 and Ser384 in the trans-activation domain of NRF1, significantly attenuated TFAM activity. Although VSV also activates TBK1, a shifting band of NRF1 was not detected in PTMSA after VSV infection. We speculate that VSV infection may specifically activate some phosphatases to antagonize TBK1-induced NRF1 phosphorylation since another RNA virus, SeV, and another DNA virus, PRV, both induced the phosphorylation of NRF1 at Ser318. It has been reported that TBK1 negatively regulates mitochondrial biogenesis via phosphorylating and inactivating AMPK in adipose tissue (Zhao *et al*, 2018). Here, we illustrate an unrecognized mechanism for the TBK1-mediated inhibition of the NRF1-TFAM axis, which is important for maintaining mtDNA stability and physiologically important to host antiviral defense.

In summary, our findings have uncovered a novel role for NRF1-mediated mitochondrial biogenesis in regulating innate antiviral immunity. Consistent with this observation, our research suggests that targeting NRF1 and mitochondrial biogenesis may help develop an efficient strategy to manipulate the processes of viral infection or autoimmune diseases.

Materials and Methods

Mice

Mice used for all the experiments were on C57BL/6J background. *Nrf1^{F/F}* and *Nrf1^{S318A/S318A}* mice were obtained from Cyagen Biosciences where they were generated by the CRISPR/Cas9-mediated genome editing. *Lyz2*-Cre mice were also provided by Cyagen Biosciences. We hybridized *Nrf1^{F/F}* mice with *Lyz2*-Cre mice to obtain myeloid-cell-specific NRF1-deficient (*Nrf1^{MyeKO}*) mice and *Nrf1^{F/F}* littermates. To create a C57BL/6J mouse model with point mutation (S318A) at mouse *Nrf1* locus, NRF1 S318A (TCG to GCA) specific gRNA targeting vector and donor oligo was designed and injected into fertilized eggs together with Cas9 mRNA for KI mouse production. A synonymous mutation at NRF1 V317 (GTG to GTT) was also introduced to prevent the binding and recutting of the sequence by gRNA after homology-directed repair. Homozygous mutation of mouse NRF1 (S318A) was confirmed by Sanger sequencing. All mice were maintained in the specific pathogen-free animal facility at the laboratory animal center of Nankai University. All animal experiments were carried out in compliance with the protocols and were approved by the Institutional Animal Care and Use Committee of Nankai University (2022-SYDWLL-000353). Samples were not blinded.

Peritoneal macrophages

Mouse peritoneal macrophages were isolated from C57BL/6J mice (6–8 weeks old) 3 days after intraperitoneal injection with the Brewer thioglycolate medium (3%, BD) and cultured in DMEM supplemented with 10% FBS.

Cell lines

HEK293T and THP-1 cells were obtained from American Type Culture Collection. Vero cells were kindly provided by Youjia Cao (Nankai University). IBMDM cells were kindly provided by Yingli Shang (Shandong Agricultural University). HEK293T, Vero, and iBMDM cells were cultured at 37°C under 5% CO_2 in DMEM supplemented with 10% FBS, 100 U/ml penicillin, and 100 μg/ml streptomycin. THP-1 cells were maintained in RPMI 1640 medium containing 10% FBS, 100 U/ml penicillin, and 100 μg/ml streptomycin. THP-1-derived macrophages were differentiated for 24 h with 100 ng/ml PMA. Cell lines were recently authenticated by STR profiling and tested for mycoplasma contamination.

Viruses

High titer stock of VSV and HSV-1 was produced in BHK-21 and Vero cells using seed stocks, respectively. All the viruses were stocked at −80°C.

Plasmids and transfection

The mammalian expression plasmids encoding Flag- or Myc-tagged wild-type human TBK1 and NRF1 were generated by PCR amplification of the corresponding cDNA followed by cloning into pFLAG-CMV-4 or pcDNA4-TO-Myc-His-B expression vectors. For recombinant His-NRF1 proteins, NRF1 was cloned into pET28a vector. All NRF1 truncations and mutations were generated based on the plasmids encoding wild-type full-length protein. The IFN-β, ISRE firefly luciferase reporter plasmids, and Renilla luciferase reporter plasmids were kindly provided by Jun Cui (Sun Yat-sen University, Guangzhou). The TFAM/NRF1-Luc and TFB1M/NRF1-Luc reporter plasmid was constructed by inserting promoter regions of TFAM or TFB1M into pGL3-basic vector. The NF-κB-Luc reporter plasmid was constructed by inserting two-times-repeated sequence of NF-κB response element into pGL3-basic vector. The primers used for reporter cloning are listed in Table EV1. Polyethylenimine (PEI, Polysciences) transfection reagent was used for all plasmids transfection. Peritoneal macrophages were transiently transfected with ISD or poly(I:C) using Lipofectamine 2000 (Invitrogen). Transfection of siRNAs into mouse peritoneal macrophages was performed by using Lipofectamine RNAiMAX (Invitrogen) with final concentrations at 50 nM (negative control siRNA, RiboBio siN05815122147; si-m-NRF1_003, RiboBio siB13122495010-1-5; si-m-Rela_001, RiboBio siB08421165522-1-5).

Reagents and pathogens

Poly(I:C) HMW (tlrl-pic), ISD Naked (tlrl-isdn), and PMA (tlrl-pma) were purchased from InvivoGen. ISD and poly(I:C) were transfected into cells and used at a final concentration of 1 μg/ml. CIP (M0290) was from NEB. MitoSOX (M36008), MitoTracker Green (M7514), MitoTracker Deep Red (M22426), and LysoTracker (L12492) were bought from Invitrogen Life Technologies. MitoQ (HY-100116A) and CsA (HY-B0579) were bought from MedChemExpress. Mouse IFN-β (439407), IL6 (431307), and TNF-α (430907) enzyme-linked immunosorbent assay (ELISA) Kits were bought from Biolegend.

VSV, Sev, and PRV were kindly provided by Yingli Shang (Shandong Agricultural University). Herpes simplex virus type 1 (HSV-1) was kindly provided by Youjia Cao (Nankai University).

Enzyme-linked immunosorbent assay (ELISA)

The concentrations of cytokines (IFN-β, IL6, and TNF-α) in cell culture supernatants and serum were measured using ELISA Kits (Biolegend) according to the manufacturer's protocols.

DNA and RNA isolation and real-time qPCR

Purification of cellular DNA was performed by using Cell/Tissue DNA Kit (Yeasen) according to the manufacturer's instructions. The ratio of mitochondrial gene (*mtAtp6* in mouse) to nuclear gene (*Tert* in mouse) was quantified by qPCR to compare mitochondrial copy numbers in different cells. Primer sequences were provided in Table EV1.

Total RNA was prepared using total RNA extraction kit (Promega). cDNA was generated using a StarScript II First-strand cDNA synthesis kit (GenStar), and quantitative real-time PCR was performed using the qPCR SYBR Green Mix (GenStar) and a

LightCycler96 real-time PCR system (Roche). Quantitation of all target gene expressions was normalized to the control gene *Gapdh* in each individual sample. The $2^{-\Delta\Delta C_t}$ method was used to calculate relative expression changes. Specific primers used in the qRT–PCR assay are listed in Table EV1.

Luciferase reporter assay

HEK293T cells were seeded in 24-well plates overnight and then transfected with luciferase reporter plasmid (200 ng), along with an internal control vector pRL-TK-Renilla luciferase (10 ng) and other expression vectors specified in the figures. After 24 h of incubation, cells were infected with VSV for another 12 h, and luciferase activities were determined using a Dual Luciferase Reporter Gene Assay Kit (Yeasen). Relative levels of luciferase activities were normalized to the levels of Renilla control.

Immunoblotting and immunoprecipitation

For immunoblot analysis, cells were lysed in lysis buffer (150 mM NaCl, 20 mM Tris, pH 7.4, 1 mM EGTA, 1 mM EDTA, 1% SDS, 2.5 mM sodium pyrophosphate, 1 mM Na_3VO_4, and protease inhibitors [Roche]). Equal amounts of proteins were separated by SDS–PAGE, electro-transferred to nitrocellulose membranes, and blocked for 1 h with 5% no-fat milk solution, followed by probing with the indicated antibodies and detection by a chemiluminescence kit (Engreen Biosystem, 29100). For Immunoprecipitation, cells were lysed in 0.5 ml IP lysis buffer (150 mM NaCl, 20 mM Tris, pH 7.4, 1 mM EGTA, 1 mM EDTA, 0.5% NP-40, 2.5 mM sodium pyrophosphate, 1 mM Na_3VO_4, and protease inhibitors [Roche]) for 1 h on a rotor at 4°C. After centrifugation at 12,000 *g* for 15 min, the supernatants were then subjected to immunoprecipitation using 2 μg specific antibodies overnight at 4°C, then protein G-agarose beads (Beyotime, P2053) were added and incubated for 3 h. The beads were then washed with the lysis buffer for 5 times. Bound proteins were eluted by boiling with loading buffer for 10 min and analyzed by SDS–PAGE. The following antibodies and dilutions were used for immunoblotting: anti-NRF1 (1:1,000, GeneTex, GTX103179), anti-NRF2-α (1:1,000, Proteintech, 21542-1-AP), anti-PGC1-α (1:1,000, Merck, ST1202, clone 4C1.3), anti-NDUFB8 (1:1,000, Proteintech, 14794-1-AP), anti-SDHA (1:1,000, Proteintech, 14865-1-AP), anti-UQCRC1 (1:1,000, Proteintech, 21705-1-AP), anti-COX IV (1:1,000, Proteintech, 11242-1-AP), anti-ATPB (1:1,000, Proteintech, 17247-1-AP), anti-mt-CO2 (1:1,000, Proteintech, 55070-1-AP), anti-TFAM (1:1,000, Proteintech, 22586-1-AP), anti-mt-ATP6 (1:1,000, ABclonal, A8193), anti-CYCS (1:1,000, BD Biosciences, 556433, clone 7H8.2C12), anti-TIMM23 (1:1,000, BD Biosciences, 611223, clone 32/Tim23), anti-HSP60 (1:5,000, BD Biosciences, 611563, clone 24/HSP60), anti-LC3 (1:1,000, MBL International, PM036), anti-Calnexin (1:5,000, Proteintech, 10427-2-AP), anti-TBK1 (1:1,000, Cell Signaling Technology, 3504, clone D1B4), anti-phospho-TBK1 (Ser172, 1:1,000, Cell Signaling Technology, 5483, clone D52C2), anti-p65 (1:1,000, Proteintech, 10745-1-AP), anti-phospho-p65 (Ser536, 1:1,000, ABclonal, AP0475), anti-STAT1 (1:1,000, Cell Signaling Technology, 14994, clone D1K9Y), anti-phospho-STAT1 (Tyr701, 1:1,000, Cell Signaling Technology, 7649, clone D4A7), anti-Flag (1:1,000, Sigma-Aldrich, F1804, clone M2), anti-Myc (1:1,000, Santa Cruz Biotechnology, sc-40, clone 9E10),

anti-β-ACTIN (1:10,000, Sigma-Aldrich, A5441, clone AC-15), anti-GAPDH (1:5,000, Proteintech, 10494-1-AP), anti-H2AFX (1:1,000, Proteintech, 10856-1-AP), anti-α-Tubulin (1:5,000, Utibody, UM4007), Anti-phosphoserine/threonine (1:1,000, Abcam, ab117253), Anti-phosphoserine (1:1,000, Abcam, ab9332), Anti-phosphothreonine (1:1,000, Abcam, ab9337). The polyclonal antibody to phosphorylated Ser318 of NRF1 was generated by Affinity Biosciences (Jiangsu) through immunization of rabbits with KLH-peptide (CNPDGTVS(P)LIQVGT) conjugate. The following antibodies were used for immunoprecipitation: anti-c-Myc (Santa Cruz Biotechnology, sc-40, clone 9E10), anti-Flag (Sigma, F1804, clone M2), and anti-TBK1 (Cell Signaling Technology, 3504, clone D1B4).

Immunofluorescence microscopy

Cells grown on glass coverslips were treated with various stimuli as indicated in the figures, then washed with PBS and fixed with 4% paraformaldehyde for 15 min at room temperature. Cells were then permeabilized with 0.1% Triton X-100 together with or without DAPI for 10 min and blocked with goat serum for 1 h. Then, the cells were incubated with primary antibodies and Alexa-labeled secondary antibodies (Invitrogen, 1:1,000) with extensive washing. Slides were then washed three times with PBS and mounted. Immunofluorescence images were obtained using a TCS SP5 Leica confocal microscope or a Zeiss LSM710 confocal microscope. The following antibodies and dilutions were used for immunofluorescence: anti-Prohibitin (1:200, Abcam, ab75766), anti-dsDNA (1:500, Abcam, ab27156), anti-HSP60 (1:1,000, BD Biosciences, 611563, clone 24/HSP60), anti-LC3 (1:500, MBL International, PM036).

Flow cytometry

To detect the differentiation and numbers of immune cells in the spleen and thymus, cells were obtained from 6-week-old $Nrf1^{MyeKO}$ mice and $Nrf1^{F/F}$ littermates, then washed with ice-cold PBS containing 1% FBS and incubated with fluorescently labeled antibody at 4°C for 30 min in the dark. Cells were then washed and resuspended in 300 μl ice-cold PBS–FBS and subjected to flow cytometry analysis on a FACS LSRII flow cytometer (BD Biosciences). FlowJo software was used for data analysis. The following antibodies were used for flow cytometry: PE anti-mouse CD3 (Biolegend, 100206, clone 17A2), FITC anti-mouse CD4 (Biolegend, 100405, clone GK1.5), APC anti-mouse CD8a (Biolegend, 100711, clone 53-6.7), APC/Cyanine7 anti-mouse CD19 (Biolegend, 115529, clone 6D5), PerCP/Cyanine5.5 anti-mouse NK1.1 (Biolegend, 108727, clone PK136), APC anti-mouse CD11b (Biolegend, 101211, M1/70), PE anti-mouse F4/80 (Biolegend, 123109, clone BM8). For analysis of mtROS in mouse PMs after the indicated stimulation, cells were collected and stained with 5 μM mitoSOX for 20 min at 37°C before flow cytometry. For analysis of mitochondrial status in mouse PMs after viral infection, cells were collected and stained with MitoTracker Green (50 nM) and MitoTracker Deep Red (50 nM) for 30 min at 37°C prior to flow cytometry.

Native PAGE

For analysis of NRF1 dimerization, cells were lysed in native lysis buffer (50 mM Tris–HCl, pH 7.4, 150 mM NaCl, 0.5% NP-40, and

100 μM PMSF). Cell lysates were centrifuged at 12,000 g for 10 min and 15 μg proteins in the supernatant were mixed with 2 × Native loading buffer (125 mM Tris–HCl, pH 6.8; 30% glycerol; and 0.1% bromophenol blue) and applied to the native gel at 4°C. 7.5% native PAGE gel without SDS was prerun with the running buffer (25 mM Tris–HCl, 192 mM glycine, in the presence of or absence of 1% deoxycholate in the cathode and anode buffer, respectively) at 40 mA for 30 min. Samples were electrophoresed at 25 mA for 40 min and were transferred to nitrocellulose membranes for immunoblotting. For analysis of mitochondrial respiratory complexes, cells were lysed in 1% digitonin (50 mM HEPES, pH 7.4, 150 mM NaCl, and 10 mg/ml digitonin). Cell lysates were centrifuged at 12,000 g for 10 min and 15 μg proteins in the supernatant were mixed with 4× Native loading buffer (Invitrogen, BN20032) for native PAGE. Native PAGE Bis-Tris Gels (Invitrogen, BN1004BOX) were used for electrophoresis according to the manufacturer's instructions.

Protein purification and *in vitro* kinase assay

His-NRF1 plasmids were transformed into *Escherichia coli* strain BL21, which were induced with IPTG (0.1 mM) at 17°C for 16 h. For His-NRF1 purification, the cell pellet was collected and resuspended in binding buffer (20 mM Tris–HCl, pH 7.4, 500 mM NaCl, 4 mM imidazole, and 1 mM PMSF). After sonication and centrifugation, the supernatant of the cell lysate was incubated with Ni^{2+}-chelating agarose beads (GE Healthcare). Beads were washed four times with washing buffer (20 mM Tris–HCl, pH 7.4, 500 mM NaCl, and 20 mM imidazole). Purified proteins were eluted in elution buffer (20 mM Tris–HCl, pH 7.4, 500 mM NaCl, and 500 mM imidazole), and then stored at −80°C after dialysis. To detect the phosphorylation of NRF1 *in vitro*, immunoprecipitated Flag-TBK1 were incubated with purified His-NRF1 in TBK1 kinase buffer (25 mM Tris–HCl, pH 7.5, 10 mM $MgCl_2$ and 1 mM DTT) containing 100 μM ATP at 30°C for 30 min. The reaction was stopped by the addition of SDS-loading buffer and subjected to SDS–PAGE and immunoblot analysis.

Viral infection and plaque assay

HEK293T, THP-1, iBMDM, and PMs ($2–5 \times 10^5$) were plated 24 h before infection. Cells were infected with VSV (0.1 MOI), HSV-1 (1 MOI), Sev (200 HAU/ml), and PRV (0.1 MOI) for various times as indicated in the figures. Viral replication was analyzed by qRT–PCR assay as described. The sequences of primers are listed in Table EV1. For plaque assay, the supernatants from cultured cells or tissue lysates from infected mice were serially diluted and used to infect Vero cells cultured in 24-well plates. After 1 h of infection, the cells were washed with PBS twice and cultured in DMEM containing 5% FBS and 1% methylcellulose for 72 h. Cells were fixed with 4% paraformaldehyde for 20 min and stained with 0.1% crystal violet for 20 min. Viral titers were calculated according to the count of plaques.

Viral infection *in vivo*

For *in vivo* viral infection, 8-week-old and sex-matched wild-type and NRF1-mutant mice (myeloid-cell-specific NRF1-deficient or NRF1 S318A KI mice) were infected with VSV (4×10^7 PFU/mouse) or HSV-1 (1×10^7 PFU/mouse) by intravenous injection. Cytokine

production in the sera was measured by ELISA. To measure VSV titers in the lungs and HSV-1 titers in the brain, snap-frozen tissues were weighed and homogenized in DMEM. The suspensions were then centrifuged and the supernatants were collected for plaque assays. The cytokines expression and viral replication in the lung and brain were determined by qRT–PCR assay as described. For survival experiments, mice were monitored for survival after infection with HSV-1. Lungs from control or VSV-infected mice were dissected, fixed in 10% phosphate-buffered formalin, embedded into paraffin, sectioned, stained with hematoxylin–eosin solution, and analyzed by light microscopy for histological changes.

Measurement of cytosolic mitochondrial DNA

Mitochondrial DNA in the cytosolic fraction was detected according to a previous protocol (Bronner & O'Riordan, 2016). Briefly, cells were lysed in a mild buffer (50 mM HEPES, pH 7.4, 150 mM NaCl, and 25 μg/ml digitonin) for 10 min at 4°C. Then, cell lysates were centrifuged at 980 g for 3 min three times to pellet intact cells. The first pellet was used for immunoblotting analysis. The cytosolic supernatants were transferred to fresh tubes and spun at 17,000 g for 10 min to isolate cytosolic preparations free of mitochondria. DNA was then purified from these pure cytosolic fractions using Cell/Tissue DNA Kit (Yeasen). Quantitative PCR was performed to analyze relative cytosolic mtDNA changes in different samples. The primers used in this detection are provided in Table EV1.

Quantification of cytosolic mtDNA by immunostaining

Fixed cells were stained with anti-DNA and anti-Prohibitin antibodies to label the mtDNA and mitochondria separately. Images were acquired on a Zeiss LSM710 confocal microscope. Thirty cells in each group were analyzed for quantification of cytosolic mtDNA. mtDNA puncta not surrounded by Prohibitin was considered as cytosolic mtDNA. The number of cytosolic mtDNA in control or experimental groups was then normalized.

RNA-seq analysis

Mouse peritoneal macrophages were isolated and infected with VSV for 8 h. Total RNA was prepared with RNA extraction kit and subjected to commercial RNA-seq analyses (Novogene) on an Illumina-HiSeq 4000 Sequencer with 150-bp paired-end reads. Reads were aligned to mouse genome mm10 using HISAT2. Bam files were sorted and indexed in SAMtools. Quantification and normalization were performed in StringTie. Differentially expressed genes (DEGs) were identified using the DESeq2. Genes with a Log_2 (fold change) > 0.5 and adjusted P value < 0.05 (as labeled in the figure captions) were considered to be significantly differentially expressed. Pathway enrichment analysis of DEGs was analyzed using the GO database and shown in Table EV2.

Electron microscopy

For ultrastructural analysis, mouse peritoneal macrophages infected with or without viruses were fixed with 2.5% glutaraldehyde in 0.1 M phosphate buffer (PB) (pH 7.4) for 15 min at 4°C. After washing with PB buffer for three times, cells were postfixed in 1% OsO_4

prepared using 0.1 M PB for 2 h at 4°C. After three washes in PB buffer, cells were dehydrated with graded series of cold ethanol (30, 50, 70, 80, 85, 90, 95, and 100%) and infiltrated sequentially in 2:1 (v:v) acetone/epoxy resin (8 h), 1:1 (v:v) acetone/epoxy resin (overnight), 100% fresh epoxy resin (8 h) at 37°C, and finally 100% fresh epoxy resin (48 h) at 60°C for polymerization. Ultrathin sections were then stained with uranyl acetate and lead citrate and observed using a Hitachi TEM operated at 80 kV.

EMSA

Nuclear extracts were prepared by using nuclear and cytoplasmic extraction kit (Beyotime Biotechnology, P0027) according to the manufacturer's instructions. Biotin–NBE (NRF1 binding element) probe (5′-biotin-TACGCTCTCCCGCGCCTGCGCCAATTCCGCC-3′, double-stranded) and biotin–NBE mutant probe (5′-biotin- TACGCTCTCCG AAAATGAAAACAATTCCGCC-3′, double-stranded) were synthesized. Nuclear extracts and DNA probe were incubated at room temperature for 20 min in a mixture containing 10 μg nuclear extract, 5× gel shift binding buffer, and 100 fmol biotin-labeled probe. Reaction products were subjected to electrophoresis with native PAGE gel and transferred to IMMOBILON-NY$^+$ membrane. The membrane was sequentially incubated with a blocking buffer for 1 h, followed by probing with streptavidin–horseradish peroxidase and detection by a chemiluminescence staining kit.

Seahorse

The oxygen consumption rate (OCR) was measured using the Seahorse XFe24 FluxPak (102342-100, Agilent) and the Seahorse XFe Analyzer (Agilent). 5×10^4 PMs were cultivated in XFe24 microplates for 24 h and then stimulated with or without VSV. Before the analysis, DMEM was replaced with XF base medium supplemented with 25 mM glucose, 2 mM glutamine, and 1 mM sodium pyruvate. Cells were then incubated in CO_2-free conditions for 1 h at 37°C, followed by the sequential addition of 1 μM Oligomycin, 4 μM FCCP and 1 μM Rotenone. The basal OCR was calculated by the last rate measurement before injection minus the nonmitochondrial respiratory rate. The maximal OCR was calculated by the maximal rate measurement after FCCP injection minus the nonmitochondrial respiratory rate.

Statistics

For graphs, all data were analyzed using Microsoft Excel 2019 or GraphPad Prism 8. Statistical analyses were conducted with a two-tailed unpaired Student's *t*-test. Survival curves were compared using the two-tailed log-rank test. All data represent the mean ± s.e.m of three independent experiments/samples unless otherwise specified. $P < 0.05$ was considered statistically significant.

Data availability

RNA-Seq data: Gene Expression Omnibus GSE218960. Source data are provided in this paper.

Expanded View for this article is available online.

Author contributions

Yushan Zhu: Conceptualization; resources; supervision; funding acquisition; methodology; writing – original draft; project administration; writing – review and editing. **Tian Zhao:** Formal analysis; investigation; writing – original draft; project administration. **Jiaojiao zhang:** Formal analysis; investigation; project administration; writing – review and editing. **Hong Lei:** Formal analysis; investigation; project administration; writing – review and editing. **Yuanyuan Meng:** Formal analysis; investigation; methodology; project administration. **Hongcheng Cheng:** Formal analysis; investigation; project administration. **Yanping Zhao:** Formal analysis; investigation; methodology. **Guangfeng Geng:** Formal analysis; investigation; project administration. **Chenlong Mu:** Formal analysis; investigation; project administration. **Linbo Chen:** Formal analysis; investigation; project administration. **Qiangqiang Liu:** Resources; methodology. **Qian Luo:** Resources; methodology. **Chuanmei Zhang:** Resources; methodology. **Yijia Long:** Resources; methodology. **Jingyi Su:** Resources; methodology. **Guo Chen:** Formal analysis; methodology. **Yanjun Li:** Resources; methodology. **Xudong Liao:** Resources; methodology. **Quan Chen:** Formal analysis; methodology. **Yingli Shang:** Resources; methodology. **Gang Hu:** Formal analysis; methodology. **Yinhao Wang:** Resources; methodology. **Zhuoya Li:** Resources; methodology. **Jiaxing Sun:** Resources; methodology.

Disclosure and competing interests statement

The authors declare that they have no conflict of interest.

References

Attardi G, Schatz G (1988) Biogenesis of mitochondria. *Annu Rev Cell Biol* 4: 289–333

Beck MA, Fischer H, Grabner LM, Groffics T, Winter M, Tangermann S, Meischel T, Zaussinger-Haas B, Wagner P, Fischer C *et al* (2021) DNA hypomethylation leads to cGAS-induced autoinflammation in the epidermis. *EMBO J* 40: e108234

Bronner DN, O'Riordan MX (2016) Measurement of mitochondrial DNA release in response to ER stress. *Bio Protoc* 6: e1839

Burman JL, Pickles S, Wang C, Sekine S, Vargas JNS, Zhang Z, Youle AM, Nezich CL, Wu X, Hammer JA *et al* (2017) Mitochondrial fission facilitates the selective mitophagy of protein aggregates. *J Cell Biol* 216: 3231–3247

Chen S, Liu S, Wang J, Wu Q, Wang A, Guan H, Zhang Q, Zhang D, Wang X, Song H *et al* (2020) TBK1-mediated DRP1 targeting confers nucleic acid sensing to reprogram mitochondrial dynamics and physiology. *Mol Cell* 80: 810–827.e7

Chernyak BV, Izyumov DS, Lyamzaev KG, Pashkovskaya AA, Pletjushkina OY, Antonenko YN, Sakharov DV, Wirtz KW, Skulachev VP (2006) Production of

reactive oxygen species in mitochondria of HeLa cells under oxidative stress. *Biochim Biophys Acta* 1757: 525–534

Cho DH, Kim JK, Jo EK (2020) Mitophagy and innate immunity in infection. *Mol Cells* 43: 10–22

Chow HM, Cheng A, Song X, Swerdel MR, Hart RP, Herrup K (2019) ATM is activated by ATP depletion and modulates mitochondrial function through NRF1. *J Cell Biol* 218: 909–928

Chung KW, Dhillon P, Huang S, Sheng X, Shrestha R, Qiu C, Kaufman BA, Park J, Pei L, Baur J *et al* (2019) Mitochondrial damage and activation of the STING pathway Lead to renal inflammation and fibrosis. *Cell Metab* 30: 784–799.e5

Domcke S, Bardet AF, Adrian Ginno P, Hartl D, Burger L, Schubeler D (2015) Competition between DNA methylation and transcription factors determines binding of NRF1. *Nature* 528: 575–579

Eichner LJ, Giguere V (2011) Estrogen related receptors (ERRs): a new dawn in transcriptional control of mitochondrial gene networks. *Mitochondrion* 11: 544–552

Elliott EI, Sutterwala FS (2015) Initiation and perpetuation of NLRP3 inflammasome activation and assembly. *Immunol Rev* 265: 35–52

Guan J, Lu C, Jin Q, Lu H, Chen X, Tian L, Zhang Y, Ortega J, Zhang J, Siteni S *et al* (2021) MLH1 deficiency-triggered DNA hyperexcision by exonuclease 1 activates the cGAS-STING pathway. *Cancer Cell* 39: 109–121.e5

Gugneja S, Scarpulla RC (1997) Serine phosphorylation within a concise amino-terminal domain in nuclear respiratory factor 1 enhances DNA binding. *J Biol Chem* 272: 18732–18739

Hartlova A, Erttmann SF, Raffi FA, Schmalz AM, Resch U, Anugula S, Lienenklaus S, Nilsson LM, Kroger A, Nilsson JA *et al* (2015) DNA damage primes the type I interferon system via the cytosolic DNA sensor STING to promote anti-microbial innate immunity. *Immunity* 42: 332–343

Hayden MS, Ghosh S (2008) Shared principles in NF-kappaB signaling. *Cell* 132: 344–362

Hayden MS, West AP, Ghosh S (2006) NF-kappaB and the immune response. *Oncogene* 25: 6758–6780

He X, Zhu Y, Zhang Y, Geng Y, Gong J, Geng J, Zhang P, Zhang X, Liu N, Peng Y *et al* (2019) RNF34 functions in immunity and selective mitophagy by targeting MAVS for autophagic degradation. *EMBO J* 38: e100978

Heo JM, Ordureau A, Paulo JA, Rinehart J, Harper JW (2015) The PINK1-PARKIN mitochondrial ubiquitylation pathway drives a program of OPTN/NDP52 recruitment and TBK1 activation to promote Mitophagy. *Mol Cell* 60: 7–20

Heo JM, Ordureau A, Swarup S, Paulo JA, Shen K, Sabatini DM, Harper JW (2018) RAB7A phosphorylation by TBK1 promotes mitophagy via the PINK-PARKIN pathway. *Sci Adv* 4: eaav0443

Humphries F, Shmuel-Galia L, Ketelut-Carneiro N, Li S, Wang B, Nemmara VV, Wilson R, Jiang Z, Khalighinejad F, Muneeruddin K *et al* (2020) Succination inactivates gasdermin D and blocks pyroptosis. *Science* 369: 1633–1637

Kelly DP, Scarpulla RC (2004) Transcriptional regulatory circuits controlling mitochondrial biogenesis and function. *Genes Dev* 18: 357–368

Khan M, Syed GH, Kim SJ, Siddiqui A (2016) Hepatitis B virus-induced Parkin-dependent recruitment of linear ubiquitin assembly complex (LUBAC) to mitochondria and attenuation of innate immunity. *PLoS Pathog* 12: e1005693

Kim SJ, Khan M, Quan J, Till A, Subramani S, Siddiqui A (2013) Hepatitis B virus disrupts mitochondrial dynamics: induces fission and mitophagy to attenuate apoptosis. *PLoS Pathog* 9: e1003722

Kim SJ, Syed GH, Khan M, Chiu WW, Sohail MA, Gish RG, Siddiqui A (2014) Hepatitis C virus triggers mitochondrial fission and attenuates apoptosis to promote viral persistence. *Proc Natl Acad Sci USA* 111: 6413–6418

Kornberg MD, Bhargava P, Kim PM, Putluri V, Snowman AM, Putluri N, Calabresi PA, Snyder SH (2018) Dimethyl fumarate targets GAPDH and aerobic glycolysis to modulate immunity. *Science* 360: 449–453

Lee KM, Giltnane JM, Balko JM, Schwarz LJ, Guerrero-Zotano AL, Hutchinson KE, Nixon MJ, Estrada MV, Sanchez V, Sanders ME *et al* (2017) MYC and MCL1 cooperatively promote chemotherapy-resistant breast cancer stem cells via regulation of mitochondrial oxidative phosphorylation. *Cell Metab* 26: 633–647.e7

Lei Y, Wen H, Yu Y, Taxman DJ, Zhang L, Widman DG, Swanson KV, Wen KW, Damania B, Moore CB *et al* (2012) The mitochondrial proteins NLRX1 and TUFM form a complex that regulates type I interferon and autophagy. *Immunity* 36: 933–946

Li T, Chen ZJ (2018) The cGAS-cGAMP-STING pathway connects DNA damage to inflammation, senescence, and cancer. *J Exp Med* 215: 1287–1299

Li XD, Sun L, Seth RB, Pineda G, Chen ZJ (2005) Hepatitis C virus protease NS3/4A cleaves mitochondrial antiviral signaling protein off the mitochondria to evade innate immunity. *Proc Natl Acad Sci USA* 102: 17717–17722

Li S, Wang J, Zhou A, Khan FA, Hu L, Zhang S (2016) Porcine reproductive and respiratory syndrome virus triggers mitochondrial fission and mitophagy to attenuate apoptosis. *Oncotarget* 7: 56002–56012

Li W, Li Y, Siraj S, Jin H, Fan Y, Yang X, Huang X, Wang X, Wang J, Liu L *et al* (2019) FUN14 domain-containing 1-mediated mitophagy suppresses hepatocarcinogenesis by inhibition of inflammasome activation in mice. *Hepatology* 69: 604–621

Liu L, Li Y, Wang J, Zhang D, Wu H, Li W, Wei H, Ta N, Fan Y, Liu Y *et al* (2021a) Mitophagy receptor FUNDC1 is regulated by PGC-1alpha/NRF1 to fine tune mitochondrial homeostasis. *EMBO Rep* 22: e50629

Liu R, Li J, Shao J, Lee JH, Qiu X, Xiao Y, Zhang B, Hao Y, Li M, Chen Q (2021b) Innate immune response orchestrates phosphoribosyl pyrophosphate synthetases to support DNA repair. *Cell Metab* 33: 2076–2089.e9

Lu Y, Ding W, Wang B, Wang L, Kan H, Wang X, Wang D, Zhu L (2020) Positive regulation of human PINK1 and Parkin gene expression by nuclear respiratory factor 1. *Mitochondrion* 51: 22–29

Luo CT, Osmanbeyoglu HU, Do MH, Bivona MR, Toure A, Kang D, Xie Y, Leslie CS, Li MO (2017) Ets transcription factor GABP controls T cell homeostasis and immunity. *Nat Commun* 8: 1062

Ma B, Cheng H, Mu C, Geng G, Zhao T, Luo Q, Ma K, Chang R, Liu Q, Gao R *et al* (2019) The SIAH2-NRF1 axis spatially regulates tumor microenvironment remodeling for tumor progression. *Nat Commun* 10: 1034

Mills EL, Kelly B, O'Neill LAJ (2017) Mitochondria are the powerhouses of immunity. *Nat Immunol* 18: 488–498

Mills EL, Ryan DG, Prag HA, Dikovskaya D, Menon D, Zaslona Z, Jedrychowski MP, Costa ASH, Higgins M, Hams E *et al* (2018) Itaconate is an anti-inflammatory metabolite that activates Nrf2 via alkylation of KEAP1. *Nature* 556: 113–117

Mohrin M, Shin J, Liu Y, Brown K, Luo H, Xi Y, Haynes CM, Chen D (2015) Stem cell aging. A mitochondrial UPR-mediated metabolic checkpoint regulates hematopoietic stem cell aging. *Science* 347: 1374–1377

Nakahira K, Haspel JA, Rathinam VA, Lee SJ, Dolinay T, Lam HC, Englert JA, Rabinovitch M, Cernadas M, Kim HP *et al* (2011) Autophagy proteins regulate innate immune responses by inhibiting the release of mitochondrial DNA mediated by the NALP3 inflammasome. *Nat Immunol* 12: 222–230

Palikaras K, Tavernarakis N (2014) Mitochondrial homeostasis: the interplay between mitophagy and mitochondrial biogenesis. *Exp Gerontol* 56: 182–188

Palikaras K, Lionaki E, Tavernarakis N (2018) Mechanisms of mitophagy in cellular homeostasis, physiology and pathology. *Nat Cell Biol* 20: 1013–1022

Palmer N, Talib SZA, Ratnacaram CK, Low D, Bisteau X, Lee JHS, Pfeiffenberger E, Wollmann H, Tan JHL, Wee S *et al* (2019) CDK2 regulates the NRF1/Ehmt1 axis during meiotic prophase I. *J Cell Biol* 218: 2896–2918

Pellegrino MW, Nargund AM, Kirienko NV, Gillis R, Fiorese CJ, Haynes CM (2014) Mitochondrial UPR-regulated innate immunity provides resistance to pathogen infection. *Nature* 516: 414–417

Satoh J, Kawana N, Yamamoto Y (2013) Pathway analysis of ChIP-Seq-based NRF1 target genes suggests a logical hypothesis of their involvement in the pathogenesis of neurodegenerative diseases. *Gene Regul Syst Bio* 7: 139–152

Scarpulla RC (1996) Nuclear respiratory factors and the pathways of nuclear-mitochondrial interaction. *Trends Cardiovasc Med* 6: 39–45

Scarpulla RC (2008) Transcriptional paradigms in mammalian mitochondrial biogenesis and function. *Physiol Rev* 88: 611–638

Scarpulla RC (2012) Nucleus-encoded regulators of mitochondrial function: integration of respiratory chain expression, nutrient sensing and metabolic stress. *Biochim Biophys Acta* 1819: 1088–1097

Scarpulla RC, Vega RB, Kelly DP (2012) Transcriptional integration of mitochondrial biogenesis. *Trends Endocrinol Metab* 23: 459–466

Seth RB, Sun L, Ea CK, Chen ZJ (2005) Identification and characterization of MAVS, a mitochondrial antiviral signaling protein that activates NF-kappaB and IRF 3. *Cell* 122: 669–682

Sprenger H-G, Langer T (2019) The good and the bad of mitochondrial breakups. *Trends Cell Biol* 29: 888–900

Stroud DA, Surgenor EE, Formosa LE, Reljic B, Frazier AE, Dibley MG, Osellame LD, Stait T, Beilharz TH, Thorburn DR *et al* (2016) Accessory subunits are integral for assembly and function of human mitochondrial complex I. *Nature* 538: 123–126

Suliman HB, Sweeney TE, Withers CM, Piantadosi CA (2010) Co-regulation of nuclear respiratory factor-1 by NFkappaB and CREB links LPS-induced inflammation to mitochondrial biogenesis. *J Cell Sci* 123: 2565–2575

Takeuchi O, Akira S (2009) Innate immunity to virus infection. *Immunol Rev* 227: 75–86

Takeuchi O, Akira S (2010) Pattern recognition receptors and inflammation. *Cell* 140: 805–820

Tannahill GM, Curtis AM, Adamik J, Palsson-McDermott EM, McGettrick AF, Goel G, Frezza C, Bernard NJ, Kelly B, Foley NH *et al* (2013) Succinate is an inflammatory signal that induces IL-1beta through HIF-1alpha. *Nature* 496: 238–242

Vega RB, Huss JM, Kelly DP (2000) The coactivator PGC-1 cooperates with peroxisome proliferator-activated receptor alpha in transcriptional control of nuclear genes encoding mitochondrial fatty acid oxidation enzymes. *Mol Cell Biol* 20: 1868–1876

Vercauteren K, Gleyzer N, Scarpulla RC (2008) PGC-1-related coactivator complexes with HCF-1 and NRF-2beta in mediating NRF-2(GABP)-dependent respiratory gene expression. *J Biol Chem* 283: 12102–12111

Virbasius JV, Scarpulla RC (1994) Activation of the human mitochondrial transcription factor a gene by nuclear respiratory factors: a potential regulatory link between nuclear and mitochondrial gene expression in organelle biogenesis. *Proc Natl Acad Sci USA* 91: 1309–1313

Virbasius CA, Virbasius JV, Scarpulla RC (1993) NRF-1, an activator involved in nuclear-mitochondrial interactions, utilizes a new DNA-binding domain conserved in a family of developmental regulators. *Genes Dev* 7: 2431–2445

Wang L, Yang L, Wang C, Zhao W, Ju Z, Zhang W, Shen J, Peng Y, An C, Luu YT *et al* (2020) Inhibition of the ATM/Chk2 axis promotes cGAS/STING signaling in ARID1A-deficient tumors. *J Clin Invest* 130: 5951–5966

Weinberg SE, Sena LA, Chandel NS (2015) Mitochondria in the regulation of innate and adaptive immunity. *Immunity* 42: 406–417

West AP, Koblansky AA, Ghosh S (2006) Recognition and signaling by toll-like receptors. *Annu Rev Cell Dev Biol* 22: 409–437

West AP, Khoury-Hanold W, Staron M, Tal MC, Pineda CM, Lang SM, Bestwick M, Duguay BA, Raimundo N, MacDuff DA *et al* (2015) Mitochondrial DNA stress primes the antiviral innate immune response. *Nature* 520: 553–557

Xu Y, Shen J, Ran Z (2020) Emerging views of mitophagy in immunity and autoimmune diseases. *Autophagy* 16: 3–17

Xu J, Cai Y, Ma Z, Jiang B, Liu W, Cheng J, Guo N, Wang Z, Sealy JE, Song C *et al* (2021) The RNA helicase DDX5 promotes viral infection via regulating N6-methyladenosine levels on the DHX58 and NFkappaB transcripts to dampen antiviral innate immunity. *PLoS Pathog* 17: e1009530

Zhang Q, Cao X (2019) Epigenetic regulation of the innate immune response to infection. *Nat Rev Immunol* 19: 417–432

Zhang Q, Raoof M, Chen Y, Sumi Y, Sursal T, Junger W, Brohi K, Itagaki K, Hauser CJ (2010) Circulating mitochondrial DAMPs cause inflammatory responses to injury. *Nature* 464: 104–107

Zhang Y, Yao Y, Qiu X, Wang G, Hu Z, Chen S, Wu Z, Yuan N, Gao H, Wang J *et al* (2019) *Listeria* hijacks host mitophagy through a novel mitophagy receptor to evade killing. *Nat Immunol* 20: 433–446

Zhao P, Wong KI, Sun X, Reilly SM, Uhm M, Liao Z, Skorobogatko Y, Saltiel AR (2018) TBK1 at the crossroads of inflammation and energy homeostasis in adipose tissue. *Cell* 172: 731–743.e12

Zhong Z, Umemura A, Sanchez-Lopez E, Liang S, Shalapour S, Wong J, He F, Boassa D, Perkins G, Ali SR *et al* (2016) NF-kappaB restricts inflammasome activation via elimination of damaged mitochondria. *Cell* 164: 896–910

Zhong Z, Liang S, Sanchez-Lopez E, He F, Shalapour S, Lin XJ, Wong J, Ding S, Seki E, Schnabl B *et al* (2018) New mitochondrial DNA synthesis enables NLRP3 inflammasome activation. *Nature* 560: 198–203

Zhou R, Yazdi AS, Menu P, Tschopp J (2011) A role for mitochondria in NLRP3 inflammasome activation. *Nature* 469: 221–225

Zhu J, Li X, Cai X, Zha H, Zhou Z, Sun X, Rong F, Tang J, Zhu C, Liu X *et al* (2021) Arginine monomethylation by PRMT7 controls MAVS-mediated antiviral innate immunity. *Mol Cell* 81: 3171–3186.e8